Cell

Article

A Dual-Mechanism Antibiotic Kills Gram-Negative Bacteria and Avoids Drug Resistance

Graphical Abstract

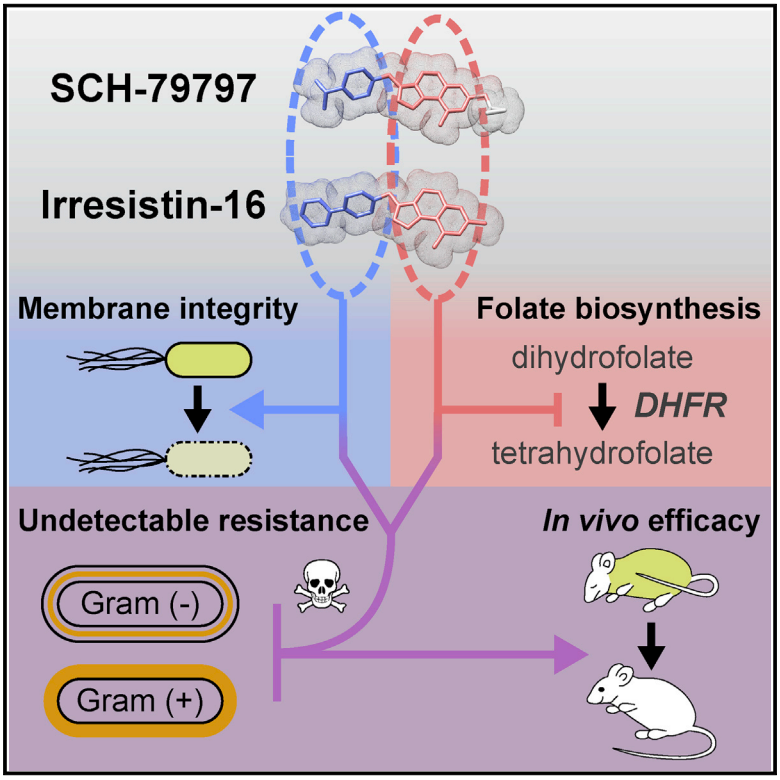

Highlights

- SCH-79797 kills Gram-negative and Gram-positive bacteria with undetectable resistance
- It works by simultaneously targeting folate metabolism and membrane integrity
- SCH's dual-targeting is synergistic, but only when on the same chemical scaffold
- Irresistin-16, an SCH derivative, effectively treats mouse *N. gonorrhoeae* infection

Authors

James K. Martin II, Joseph P. Sheehan, Benjamin P. Bratton, ..., Mikhail M. Savitski, Maxwell Z. Wilson, Zemer Gitai

Correspondence

zgitai@princeton.edu

In Brief

A compound that kills both Gram-positive and Gram-negative bacteria through two independent mechanisms may provide a platform for the development of future antibiotics.

Martin et al., 2020, Cell *181*, 1518–1532
June 25, 2020
https://doi.org/10.1016/j.cell.2020.05.005

CellPress

CellPress

Cell

Article

A Dual-Mechanism Antibiotic Kills Gram-Negative Bacteria and Avoids Drug Resistance

James K. Martin II,[1,7] Joseph P. Sheehan,[1,7] Benjamin P. Bratton,[1,2,7] Gabriel M. Moore,[1] André Mateus,[3] Sophia Hsin-Jung Li,[1] Hahn Kim,[4,5] Joshua D. Rabinowitz,[2,4] Athanasios Typas,[3] Mikhail M. Savitski,[3] Maxwell Z. Wilson,[1,6] and Zemer Gitai[1,8,*]

[1]Department of Molecular Biology, Princeton University, Princeton, NJ 08544, USA
[2]Lewis-Sigler Institute for Integrative Genomics, Princeton University, Princeton, NJ 08544, USA
[3]European Molecular Biology Laboratory, Genome Biology Unit, 69117 Heidelberg, Germany
[4]Department of Chemistry, Princeton University, Princeton, NJ 08544, USA
[5]Princeton University Small Molecule Screening Center, Princeton University, Princeton, NJ 08544, USA
[6]Department of Molecular, Cellular, and Developmental Biology, Center for BioEngineering, University of California, Santa Barbara, Santa Barbara, CA 93106, USA
[7]These authors contributed equally
[8]Lead Contact
*Correspondence: zgitai@princeton.edu
https://doi.org/10.1016/j.cell.2020.05.005

SUMMARY

The rise of antibiotic resistance and declining discovery of new antibiotics has created a global health crisis. Of particular concern, no new antibiotic classes have been approved for treating Gram-negative pathogens in decades. Here, we characterize a compound, SCH-79797, that kills both Gram-negative and Gram-positive bacteria through a unique dual-targeting mechanism of action (MoA) with undetectably low resistance frequencies. To characterize its MoA, we combined quantitative imaging, proteomic, genetic, metabolomic, and cell-based assays. This pipeline demonstrates that SCH-79797 has two independent cellular targets, folate metabolism and bacterial membrane integrity, and outperforms combination treatments in killing methicillin-resistant *Staphylococcus aureus* (MRSA) persisters. Building on the molecular core of SCH-79797, we developed a derivative, Irresistin-16, with increased potency and showed its efficacy against *Neisseria gonorrhoeae* in a mouse vaginal infection model. This promising antibiotic lead suggests that combining multiple MoAs onto a single chemical scaffold may be an underappreciated approach to targeting challenging bacterial pathogens.

INTRODUCTION

More than twenty unique classes of antibiotics were characterized in the 30 years following the discovery of penicillin in 1929 (Coates et al., 2011; Davies, 2006). However, a combination of scientific and economic factors have slowed the discovery and development of these life-saving molecules to the extent that only six new classes of antibiotics have been approved in the past 20 years, none of which are active against Gram-negative bacteria (Butler et al., 2017). This decline in the discovery of new antibiotic classes, coupled with the evolution of multi-drug resistant bacteria and horizontal transfer of resistance mechanisms, has created a public health crisis that is predicted to only escalate in the coming years (Culyba et al., 2015; Hofer, 2019; O'Neill, 2014).

Recent efforts have begun to reinvigorate antibiotics research, but most of this work has resulted in compounds that function via similar mechanisms to those of traditional antibiotics. For example, finafloxacin, a fluoroquinolone antibiotic that was recently approved to treat ear infections caused by *Pseudomonas aeruginosa*, is more effective than other fluoroquinolones because it maintains its potency in acidic environments (McKeage, 2015). However, finafloxacin is still susceptible to the same resistance mechanisms that affect other fluoroquinolones (Randall et al., 2016). The recent discovery of the natural product teixobactin suggests that it is possible to find compounds that selectively kill bacteria without being prone to resistance (Ling et al., 2015). However, teixobactin is only functional against Gram-positive bacteria. Another natural product, darobactin, was recently found to specifically target Gram-negative bacteria, but resistance to darobactin was relatively easy to achieve through mutations in *bamA* (Imai et al., 2019). Thus, there is still a strong need for characterizing new classes of antibiotics with distinct mechanisms of action (MoA), especially those that target Gram-negatives with low resistance frequency.

An ideal antibiotic would be hard to develop resistance against, able to kill both Gram-positive and Gram-negative bacteria, and easy to access. It is important to note that while antibiotics that are not prone to resistance are attractive clinically,

selecting for resistant mutants is the most common method for characterizing MoA, making the characterization of new antibiotic MoAs without resistance mutants a significant challenge. Phenotypic methods, such as macromolecular synthesis assays, have been previously used in such cases, as was done for teixobactin (Ling et al., 2015). However, these assays only allow the classification of molecules with previously described MoAs (King and Wu, 2009). Thus, there is also a need for resistance-independent approaches for the *de novo* characterization of antibiotic MoA.

Here, we describe a compound, SCH-79797, which is bactericidal toward both Gram-negative and Gram-positive bacteria, including clinically significant bacterial pathogens such as methicillin resistant *Staphylococcus aureus* (MRSA), *Enterococcus faecalis*, *Neisseria gonorrhoeae*, and *Acinetobacter baumannii*, with no signs of resistance. In an animal host model, SCH-79797 blocked infection by *A. baumannii* with low toxicity to the host at the dose required for effective antibiotic activity. To rapidly and efficiently classify the MoA of SCH-79797, we used a variant of a recently described quantitative imaging-based approach known as bacterial cytological profiling (BCP) (Nonejuie et al., 2013). This effort showed that SCH-79797 functions through a mechanism distinct from that of most known classes of antibiotics. In the absence of being able to evolve resistant mutants, we used thermal proteome profiling (Savitski et al., 2014), CRISPRi genetic sensitivity (Peters et al., 2016), and metabolomic profiling (Kwon et al., 2008; Kwon et al., 2010) to characterize the MoA of SCH-79797. Using this multi-dimensional, systems-level approach, we identified the candidate targets of SCH-79797 as dihydrofolate reductase and the bacterial membrane. Classical enzymology and membrane permeability and polarization assays confirmed the targets identified by our high-throughput approaches. By analyzing derivatives of the SCH-79797 structure, we demonstrated that the two pharmacophores of this compound can be distinguished. Finally, we describe a derivative of SCH-79797, Irresistin-16 (IRS-16), with improved potency that demonstrates efficacy in a mouse vaginal *Neisseria gonorrhoeae* model. Thus, our findings identify and characterize a promising antibiotic candidate and provide a potential roadmap for future antibiotic discovery efforts.

RESULTS

SCH-79797 Is a Broad-Spectrum, Bactericidal Antibiotic

With the aim of finding antibiotics with novel mechanisms of action (MoA), we began with an unbiased, whole-cell screening approach. To include antibiotics that target both Gram-negative and Gram-positive bacteria, we screened for compounds that inhibited the growth of *E. coli lptD4213*, which has a compromised outer membrane that makes it partially permeable to antibiotics that would otherwise have difficulty penetrating the Gram-negative lipopolysaccharide (Ruiz et al., 2006). We screened a small molecule library of ~33,000 unique compounds and one of our most potent hits was SCH-79797, a compound that had been previously reported as a human PAR-1 antagonist (Ahn et al., 2000). This finding was surprising because there are no PAR-1 homologs in bacteria. A recent report suggested that SCH-79797 increases the ability of neutrophils to kill bacteria, perhaps by directly functioning as an antibiotic (Gupta et al., 2018). Given that studies focusing on characterizing its anticoagulant activities suggested that at least 5 mg/kg SCH-79797 can be safely tolerated in animals (Gobbetti et al., 2012; Strande et al., 2007) and its emergence as a potential antimicrobial with no known bacterial target (Gupta et al., 2018), we decided to further characterize SCH-79797 as a candidate antibiotic.

To assess the spectrum of bacterial species susceptible to SCH-79797, we measured the minimal inhibitory concentration (MIC) of SCH-79797 against several clinically relevant pathogens, including the ESKAPE pathogens (Boucher et al., 2009). In this study, we define MIC as the concentration of drug that results in no visible bacterial growth after 14 h of growth at 37°C. We found that SCH-79797 significantly hindered the growth of multiple Gram-negative and Gram-positive pathogens including *Neisseria gonorrhoeae,* two clinical isolates of *Acinetobacter baumannii*, *Enterococcus faecalis*, and *Staphylococcus aureus* (Figure 1A; Table S1). SCH-79797 also exhibited potent activity against several antibiotic-resistant pathogen strains including multi-drug-resistant WHO-L *N. gonorrhoeae* and MRSA *S. aureus.* Using the *E. coli lptD4213* strain from our original screen, SCH-79797 exhibited potent and rapid bactericidal activity (Figures 1B and 1C). SCH-79797 also exhibited similar bactericidal activity against a clinical isolate of *S. aureus* MRSA USA300 (Tenover and Goering, 2009) suggesting that its bactericidal activity is not species-specific (Figure S1A).

SCH-79797 Is Effective *In Vivo* and Has a Low Frequency of Resistance

Given SCH-79797's promising ability to kill bacteria, we sought to determine if it can function as an effective antibiotic *in vivo*. To test its antibiotic activity in the context of an animal host infection, we focused on *A. baumannii* as it has emerged as an important Gram-negative pathogen that is targeted by relatively few available antibiotics, and has a well-established host animal model in the wax worm, *Galleria mellonella* (Gebhardt et al., 2015; Peleg et al., 2009). We first established that injecting *G. mellonella* with SCH-79797 at concentrations four times higher than the MIC of SCH-79797 toward *A. baumannii* did not result in higher host toxicity than the solvent-only control (Figures S1E and S1F; Table S2). We next tested the ability of SCH-79797 to treat infection of *G. mellonella* with a lethal dose of *A. baumannii* AB17978. Treatment with SCH-79797 significantly prolonged the survival of *A. baumannii*-infected *G. mellonella* ($p < 0.001$) (Figures 1D, S1G, and S1H). The survival rate of *G. mellonella* treated with SCH-79797 was similar to the control antibiotics meropenem, rifampicin, and gentamicin (Figures 1D, S1G, and S1H) (Karlowsky et al., 2003; Viehman et al., 2014).

To further characterize its promise as an antibiotic, we attempted to determine the frequency with which bacteria develop resistance toward SCH-79797. Because spontaneous suppressors can restore *E. coli lptD4213*'s membrane barrier functionality, we focused our resistance studies on *S. aureus* MRSA USA300 (Tenover and Goering, 2009). We were unable to isolate stable SCH-79797-resistant mutants upon plating ~10^8 CFU of MRSA USA300 onto agar containing 25 μg/mL SCH-79797 (4X MIC). We were also unable to isolate SCH-79797-resistant mutants upon plating ~10^8 colony-forming units (CFUs) of

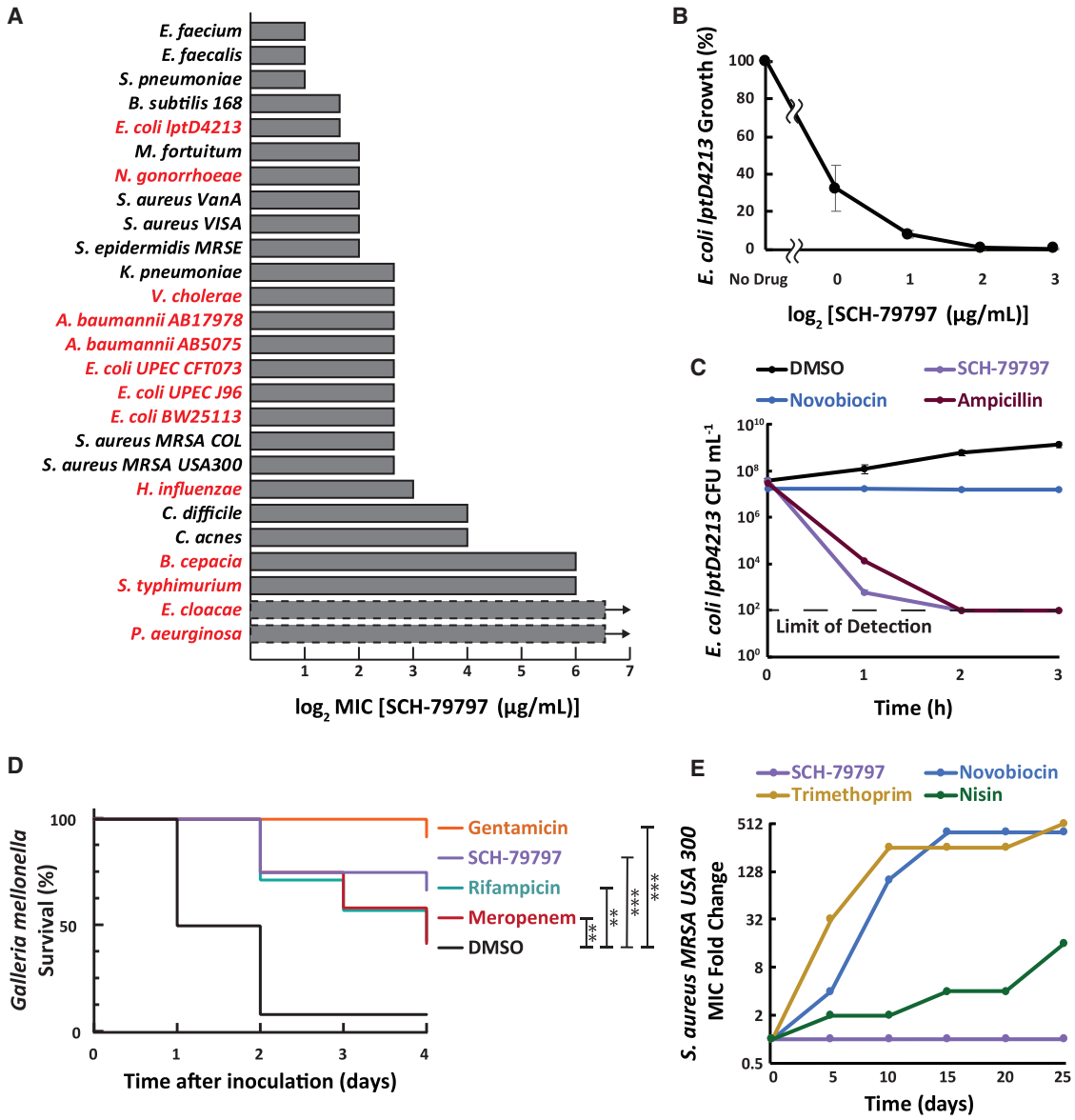

Figure 1. SCH-79797 Is a Broad-Spectrum, Bactericidal Antibiotic that Is Effective in an Animal Model and Has a Low Frequency of Resistance

(A) The MIC of SCH-79797 against Gram-negative (red) and Gram-positive (black) bacteria. The MICs of *E. cloacae and P. aeruginosa* were greater the maximal drug concentrations tested. See also Table S1.

(B) The relative growth of *E. coli lptD4213* after treatment with SCH-79797. Bacterial growth was measured as the optical density at 600 nm (OD_{600}) 14 h following inoculation. Each data point represents 2 biological replicates. Mean ± SD are shown.

(C) Colony forming units (CFUs mL^{-1}) after 3-h treatment of *E. coli lptD4213* with 1% DMSO (solvent control), 6.2 μg/mL SCH-79797 (2× MIC), 0.12 μg/mL ampicillin (2× MIC), or 0.48 μg/mL novobiocin (4× MIC). Data points at 1×10^2 CFU mL^{-1} are below the level of detection. Each data point represents 3 biological replicates. Mean ± SD are shown.

(D) The percent survival of *G. mellonella* wax worms infected with *A. baumannii* and concomitantly treated with 2 μL/larva 100% DMSO, 67 μg/larva SCH-79797, 67 μg/larva gentamicin, 67 μg/larva merapenem, or 67 μg/larva rifampicin. Data represents a typical cohort (n = 12) from a biological triplicate. p values are determined from a Mantel-Cox test using Prism (**$p < 0.01$; ***$p < 0.001$), and the pooled results are presented in the supplemental material (Figure S1G). For other Mantel-Cox comparisons, see Table S2.

(E) Fold increase in resistance of *S. aureus* MRSA USA300 to SCH-79797, novobiocin, trimethoprim, or nisin after 25 days of serial passaging in each drug. Data represents one biological replicate and the data for a second replicate is shown in Figure S1B.

B. subtilis, suggesting that the difficulty in developing resistant mutants is not species-specific. To address resistance rates more quantitatively, we serial-passaged 2 biologically independent cultures of *S. aureus* MRSA USA300 in sub-lethal concentrations of SCH-79797, as well as three control antibiotics: novobiocin, trimethoprim, and nisin. Over the course of 25 days, we

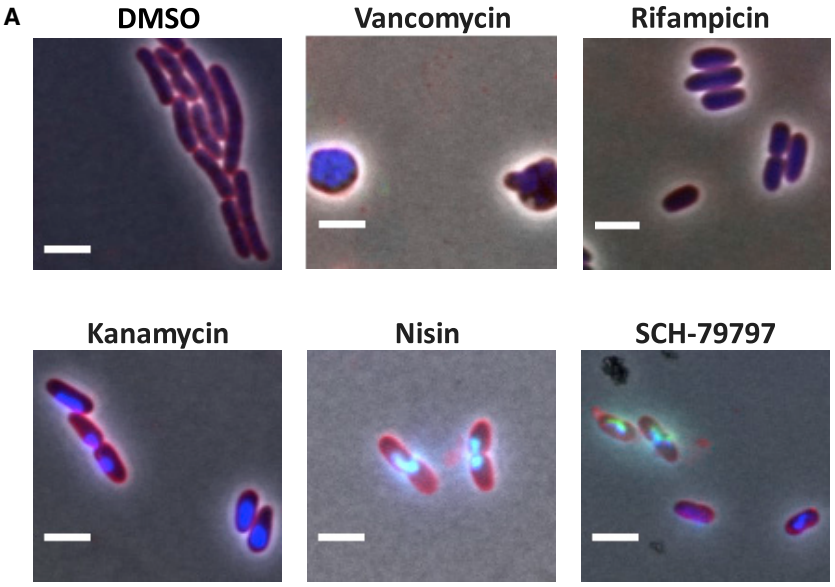

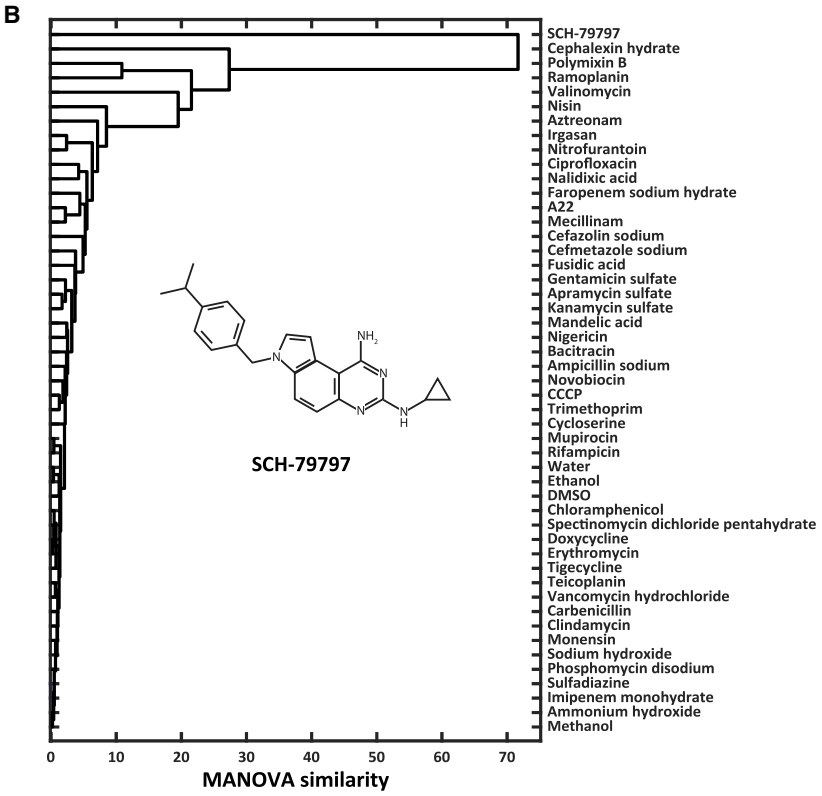

Figure 2. Bacterial Cytological Profiling Indicates that SCH-79797 Functions by a Mechanism Distinct from Known Classes of Antibiotics

(A) Fluorescent images of *E. coli lptD4213* cells treated with antibiotics representative of 5 different antibiotic classes. Cells were treated for 2 h with 5× MIC of each drug. Merged image channels are phase contrast (gray), FM4-64 (red), DAPI (blue), and SYTOX (green). Scale bar, 1 μm.

(B) Comparison of cytological profiles of known antibiotics with the cytological profile of SCH-79797. Single-linkage clustered dendrogram from one-way MANOVA comparisons between antibiotic treatment groups compared to all other antibiotic treatment groups. Inset: structure of SCH-79797.

successfully isolated mutants resistant to all the control antibiotics while no SCH-79797-resistant mutants emerged (Figures 1E and S1B). For novobiocin, trimethoprim, and nisin, resistance gradually increased throughout the experiment, while the resistance level remained constant for SCH-79797 (Figures 1E and S1B), indicating that these bacteria did not even acquire partial resistance to SCH-79797. In addition, the mutants that evolved increased resistance to antibiotics like trimethoprim and nisin did not demonstrate cross-resistance to SCH-79797 (Figure S1D). To extend these findings to a Gram-negative species, we repeated our serial passaging study with 2 biologically independent cultures of *A. baumannii* AB17978 (Figure S1C). *A. baumannii* resistance remained constant for SCH-79797 but increased for all other antibiotics, including gentamycin, supporting the conclusion that the lack of resistance to SCH-79797 is not species-specific.

A Variant of Bacterial Cytological Profiling Suggests that SCH-79797 Has a Unique MoA

The inability to isolate SCH-79797-resistant mutants makes SCH-79797 an appealing candidate antibiotic but poses a challenge for determining its MoA. As a result, we used a quantitative imaging-based approach to determine if the MoA of SCH-79797 is similar to that of any previously characterized antibiotics. Specifically, we modified a single-cell, high-content imaging methodology, known as BCP (Nonejuie et al., 2013). The logic of BCP is that antibiotics with similar MoA result in similar death phenotypes such that by quantifying how bacteria appear upon death, we can gain insight into the cause of death (much like a bacterial autopsy). Here, we applied our BCP analysis to a training set of 37 distinct antibiotics with known MoA as well as to SCH-79797. For each compound, we treated *E. coli lptD4213* with 5X MIC of an antibiotic for 2 h, stained with three dyes that report on nucleoid morphology (DAPI), membrane morphology (FM4-64), and membrane integrity (SYTOX Green), and imaged the cells at high resolution (Figure 2A). For each condition we imaged ~100 cells and quantified 14 parameters reflecting various morphological and fluorescence features (Table S3).

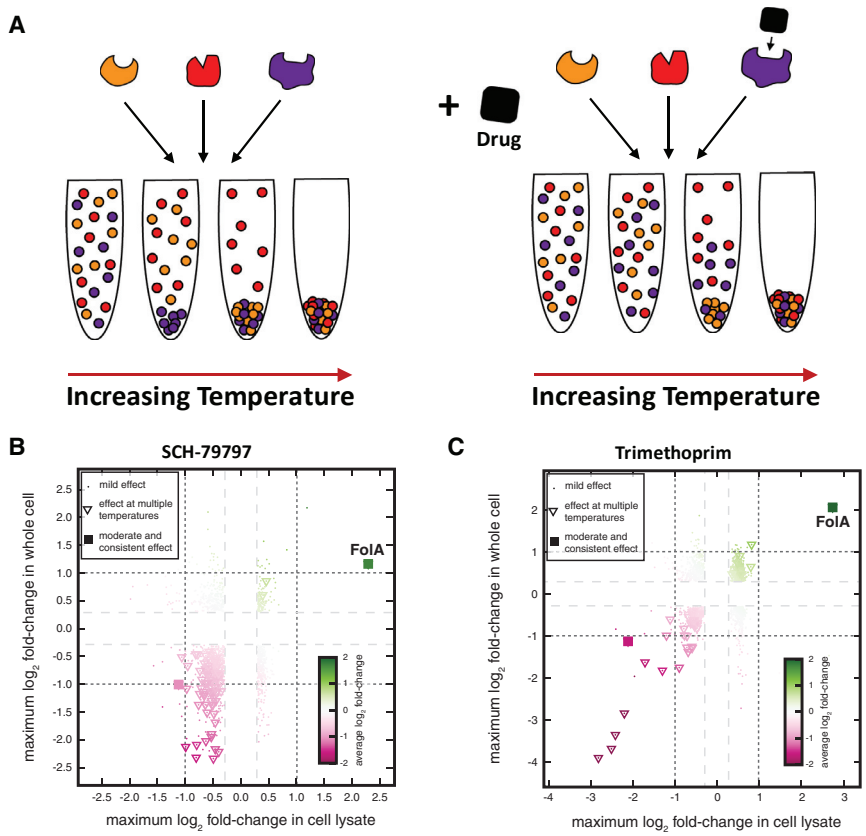

Figure 3. Thermal Proteome Profiling Suggests that SCH-79797 Binds Dihydrofolate Reductase

(A) Schematic of the thermal shift assay that compares the thermal stability of the entire proteome with and without drug treatment. Protein samples are aliquoted, and each aliquot is heated to a different temperature. The relative fraction of soluble and insoluble proteins is then determined for each aliquot by ultracentrifugation and mass spectrometry.

(B and C) The relative thermal stability of the soluble *E. coli lptD4213* proteome after treatment of whole cell and cell lysate samples with SCH-79797 (B) or trimethoprim (C). Changes in thermal stability were determined by measuring changes in the abundance of soluble protein across 10 different temperatures ranging from 42°C–72°C and 4 drug concentrations and a vehicle control. For each point, the color indicates the maximal effect size across all temperatures and the largest change in abundance across all concentrations. Squares represent the proteins with a change in abundance of at least 25% at three or more temperatures. To be considered consistent, the change in abundance of a protein had to show the same sign at least 90% of the time and have an effect size of at least 2-fold in either whole cells or cell lysates. Triangles represent a milder effect where at least one temperature had a change in abundance of at least 25% in both whole cell and cell lysate treatments.

Because we had gold standards of the BCP results of SCH-79797 and of several antibiotics representing different classes and sub-groups within classes, we applied a machine learning approach to classify the BCP data. Using a one-way MANOVA, we performed dimensionality reduction to remove the influence of naturally covarying metrics, such as cell length and cell perimeter. We then used single-linkage clustering to cluster treatment groups by their neighborhood representation vectors, such that samples whose neighborhoods were similar would be clustered together. This analysis indicated that SCH-79797 resulted in a phenotypic death-state that was different from the other antibiotics tested (Figure 2B). We also tested an additional method to assess whether this result was robust to multiple statistical methods. Using UMAP for dimensionality reduction on *Z* score normalized data (McInnes et al., 2018), we found that SCH-79797-treated cells formed a distinct peak separated from other treatments (Figure S2). This result supports our conclusion that SCH-79797 is dissimilar from most antibiotics tested and therefore likely possesses a MoA distinct from that of any of the antibiotics in our training set.

Thermal Profiling and CRISPRi Genetics Demonstrate that SCH-79797 Targets Dihydrofolate Reductase

In the absence of resistant mutants or similarity to antibiotics with known MoA by BCP, we turned to a high-throughput proteomics-based approach for *de novo* identification of candidate SCH-79797 targets. Specifically, we used thermal proteome profiling, an assay that uses mass spectrometry to compare the thermal stability of the entire proteome with and without drug treatment (schematized in Figure 3A) (Mateus et al., 2018; Savitski et al., 2014). Briefly, intact cells or cell lysate samples treated with a range of compound concentrations are heated to a series of increasing temperatures and the soluble proteins at each temperature are collected (Becher et al., 2016). Proteins that bind to the drug are thermally stabilized, which leads to a shift in the temperature at which those proteins precipitate (Figure 3A). Using *E. coli lptD4213*, we treated intact cells and cell lysates with SCH-79797 and found that it significantly shifted the thermal stability of dihydrofolate reductase (the DHFR homolog in *E. coli* is known as FolA) (Figures 3B and S3A). The fact that the same result was observed with both intact cells and cell lysates (Figures 3B and S3A) suggests that SCH-79797 enters *E. coli* cells and directly binds to FolA. As a positive control, we used a well-characterized antibiotic that targets DHFR, trimethoprim, and found that it also thermally stabilizes its known target, the *E. coli* DHFR, FolA (Figures 3C and S3B) (Gleckman et al., 1981).

To test both the physiological significance and species-specificity of the suggestion that SCH-79797 binds to DHFR, we took advantage of a collection of *B. subtilis* essential gene CRISPR-interference (CRISPRi) knockdown mutants (Peters et al., 2016). In each of these mutants, an essential gene is targeted by CRISPRi to reduce its expression ~3-fold. A strain with

reduced levels of the SCH-79797 target should be sensitized to sub-lethal doses of SCH-79797. Given the thermal profiling result, we focused on mutants in the folate biosynthesis pathway (schematized in Figure 4A). As a negative control, we confirmed that CRISPRi knockdowns of genes unrelated to folate metabolism are not sensitized to SCH-79797 (Figure S4). As a positive control for our assay, we again utilized trimethoprim. We confirmed that dihydrofolate reductase (*dfrA* in *B. subtilis*) and dihydrofolate synthase (*folC*, an enzyme that acts upstream of DfrA) knockdowns are hypersensitive to trimethoprim, while knockdowns of enzymes that function downstream of DHFR, *folD* and *glyA*, are not (Figure 4B). SCH-79797 exhibited the same genetic sensitivity pattern as trimethoprim in that both *dfrA* and *folC*, but not *folD* and *glyA* knockdowns, were sensitized to SCH-79797 (Figure 4B).

SCH-79797 Inhibits DHFR Activity in Cells and in Purified Enzymatic Assays

To determine how SCH-79797 affects folate metabolism in living cells, we used mass spectrometry to measure the relative abundance of folate metabolite pools in *E. coli* NCM3722 treated with SCH-79797. *E. coli* NCM3722 was used because these bacteria lack mutations that disrupt primary metabolism in other lab strains of *E. coli* (Soupene et al., 2003). *E. coli* NCM3722 cells were grown in Gutnick Minimal Media and treated with 13.9 μg/mL SCH-79797 (1× MIC) for 15 min (Kwon et al., 2008, 2010). In response to SCH-79797 treatment, the levels of the DHFR substrate, 7,8-dihydrofolate (DHF), rose ~10-fold compared to untreated cells, while the levels of folate metabolites downstream of DHF dropped significantly (Figure 4C). This metabolic response is characteristic of dihydrofolate reductase (FolA in *E. coli*) inhibition as we observed a similar pattern upon treatment with trimethoprim, a known inhibitor of DHFR (Figure 4C) (Gleckman et al., 1981).

To determine whether SCH-79797 inhibits DHFR directly, we obtained purified *E. coli* FolA protein and measured its enzymatic activity in the presence of increasing concentrations of SCH-79797. We found that SCH-79797 has an IC_{50} of 8.6 ± 3 μM against FolA (Figure 4D). We also measured the initial velocity of FolA activity at various DHF substrate concentrations to establish if SCH-79797 acts competitively or non-competitively. A Michaelis-Menten fit to the data demonstrated that 8.6 μM SCH-79797 (the IC_{50}) increases the K_m from 32 ± 25 μM to 100 ± 80 μM. These results indicate that SCH-79797 functions at least partially as a competitive inhibitor of FolA's activity on its DHF substrate (Figure 4E). Likewise, the Michaelis-Menten fits for the established FolA inhibitor trimethoprim show a very similar effect IC_{50} = 15 ± 4 nM (Figure 4D), consistent with previous measurements of the tight binding between trimethoprim and *E. coli* FolA (Cammarata et al., 2017).

SCH-79797 Also Disrupts Bacterial Membrane Potential and Permeability Barrier

The similarities between SCH-79797 and trimethoprim with respect to FolA inhibition helped confirm DHFR as a target of SCH-79797 but were also surprising because these two compounds did not generate similar profiles in our BCP analysis (Figure 2B). One potential explanation is that SCH-79797 has additional targets that are not shared with trimethoprim. If this was the case, we would expect that cells resistant to trimethoprim would still be susceptible to SCH-79797. Previous studies demonstrated that resistance to trimethoprim can be achieved by deleting *thyA* and supplementing the media with thymine (Amyes and Smith, 1975). We confirmed that deleting *thyA* from *E. coli lptD4213* in the presence of excess thymine led to trimethoprim resistance (Figure 5A). We also found that thymine supplementation decreased the sensitivity of *E. coli lptD4213* to SCH-79797 (comparing "WT" of Figure 5A to Figure 1B; Table S1). The findings that reducing cellular dependence on DHFR activity (by thymine supplementation) makes cells less sensitive to SCH-79797 treatment, while increasing reliance on DHFR activity (by *dfrA* CRISPRi) makes cells more sensitive to SCH-79797, together indicate that DHFR inhibition is a physiologically important target of SCH-79797. Nevertheless, comparing cells with and without *thyA* in the presence of thymine showed no change in sensitivity to SCH-79797 (Figure 5A), suggesting that SCH-79797 is likely to have a second, folate-independent MoA.

To obtain clues about the potential additional MoA of SCH-79797, we revisited our fluorescent BCP images of *E. coli lptD4213* cells treated with SCH-79797. We observed SYTOX Green staining in some of the bacteria (Figure 2A), suggesting that SCH-79797 compromises the integrity of the bacterial membrane. To directly quantify the effect of SCH-79797 on bacterial membrane integrity, we used flow cytometry to measure the membrane potential and permeability of *E. coli lptD4213* in the presence of the fluorescent dyes, $DiOC_2(3)$ and TO-PRO-3. $DiOC_2(3)$ is a cationic dye that accumulates in the cytoplasm of cells with an active membrane potential and shifts its fluorescence from red to green in these cells, providing a measure of membrane potential (Figure 5B) (Novo et al., 1999). TO-PRO-3 is a nucleic acid stain that only accumulates in cells with compromised membranes, providing an independent measure of membrane permeability (Figure 5B) (Novo et al., 2000). As positive controls, we observed the expected shifts in both $DiOC_2(3)$ and TO-PRO-3 staining using CCCP, a membrane-decoupler that affects membrane potential but not permeability (Novo et al., 2000), and two compounds that disrupt both membrane potential and permeability: nisin, a pore-forming antibacterial peptide (Prince et al., 2016; Wiedemann et al., 2001), and polymyxin B, a small lipopeptide membrane destabilizer (Warren et al., 1957) (Figure 5C). As negative controls, we confirmed that antibiotics that do not target the membrane, including ampicillin, rifampicin, and novobiocin, do not shift $DiOC_2(3)$ or TO-PRO-3 staining (Figures S5A–S5D). After 15 min of treatment with SCH-79797, subsequent $DiOC_2(3)$ and TO-PRO-3 staining revealed significant defects in both membrane polarization and permeability (Figure 5C). These effects on the membrane are not secondary consequences of DHFR inhibition, as trimethoprim-treated *E. coli* showed no significant changes in $DiOC_2(3)$ and TO-PRO-3 staining (Figure 5C). The membrane-targeting effect of SCH-79797 is also not species-specific, as similar results were seen with SCH-79797-treated *B. subtilis* 168 (Figures S5E–S5G). These findings indicate that independent of its ability to inhibit DHFR activity, SCH-79797 disrupts both membrane potential and permeability barrier.

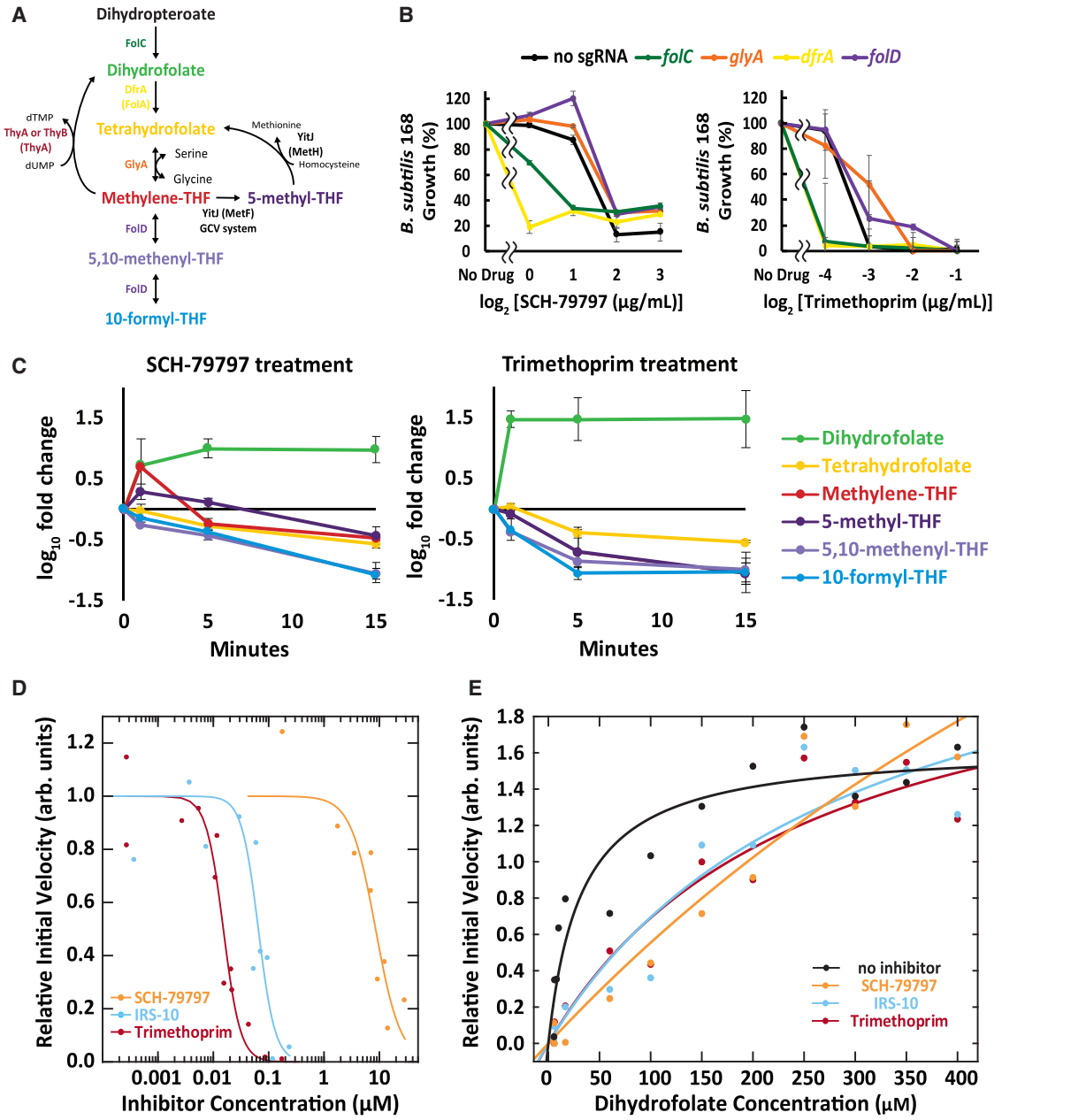

Figure 4. SCH-79797 Targets Folate Metabolism by Competitively Inhibiting Dihydrofolate Reductase

(A) A partial representation of the folate synthesis pathway. Where the *E. coli* and *B. subtilis* differ, the *E. coli* names are listed in parentheses.

(B) The growth of CRISPRi *B. subtilis* knockdown mutants (Peters et al., 2016) involved in folate synthesis relative to a DMSO-treated control after SCH-79797 or trimethoprim treatment. OD_{600} of each condition 14 h after inoculation was plotted against drug concentration. Each data point represents 2 biological replicates. Mean ± SD are shown.

(C) Metabolomic analysis of *E. coli* NCM3722 cells treated with 13.9 μg/mL SCH-79797 (1× MIC) or 0.15 μg/mL trimethoprim (1× MIC). Samples were taken 0, 5, 10, and 15 min after drug treatment. Folate metabolite abundance at each time point was quantified relative to the DMSO-treated control samples at the initial time point. Each data point represents 3 independent replicates. Mean ± SD are shown.

(D and E) *E. coli* dihydrofolate reductase (FolA) activity is reduced in the presence of SCH-79797, IRS-10, or trimethoprim. Activity is relative to the standard condition of 60 μM NADPH and 100 μM DHF. (D) IC_{50} values were derived from fits to the Hill equation for reactions performed at 60 μM NADPH and 100 μM DHF. (E) FolA activity as a function of dihydrofolate concentration in the presence of 8.6 μM SCH-79797 (IC_{50}), 0.065 μM IRS-10 (IC_{50}), or 0.015 μM trimethoprim (IC_{50}). Kinetic parameters are derived from fits to the Michaelis-Menten model.

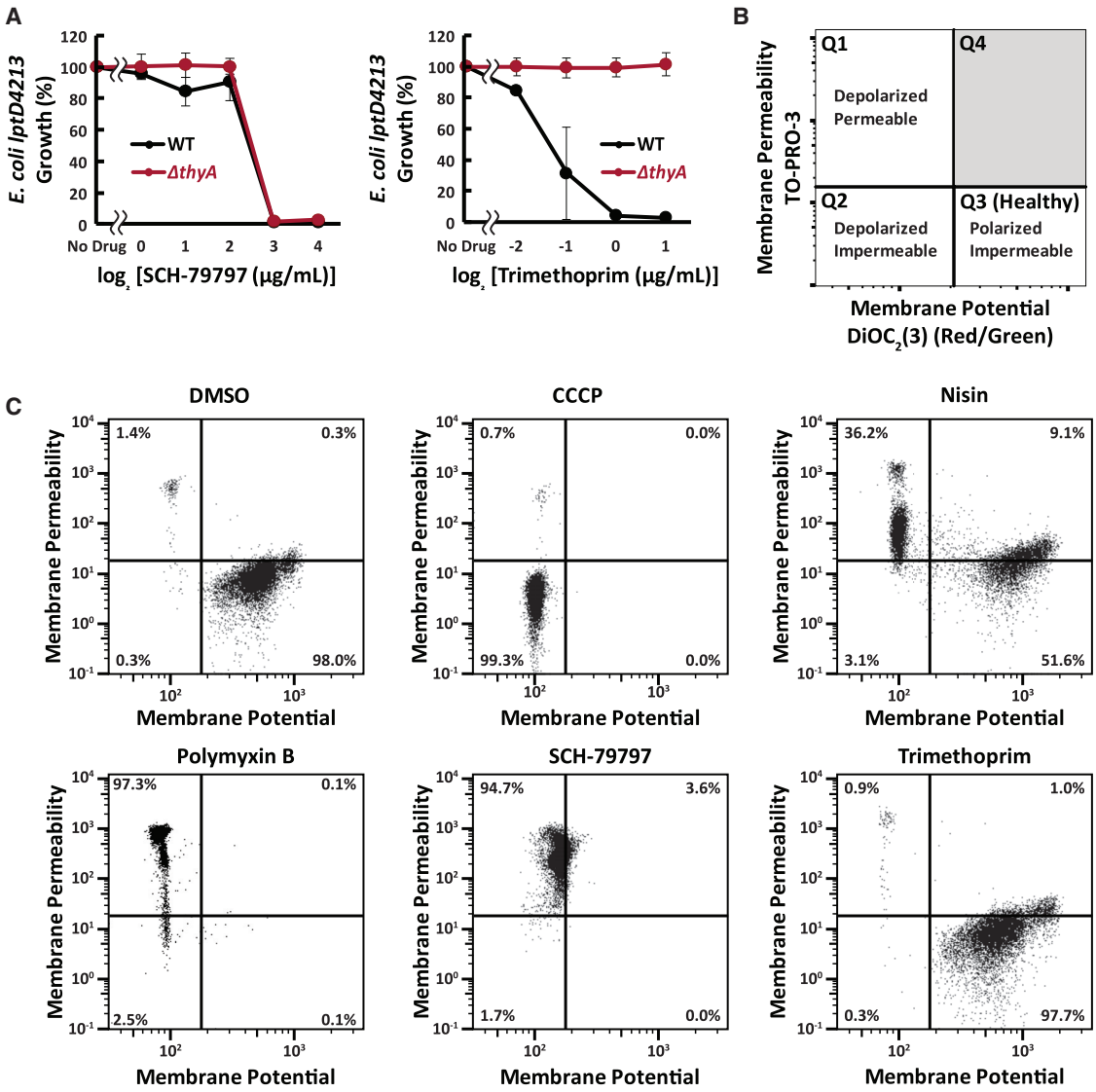

Figure 5. SCH-79797 Is Distinct from Other Dihydrofolate Reductase Inhibitors and Disrupts Membrane Integrity

(A) The growth of wild-type (WT) and Δ*thyA E. coli lptD4213* relative to a DMSO-treated control after SCH-79797 and trimethoprim treatment. Bacterial growth was measured for 14 h and the final OD_{600} of each condition was plotted against drug concentration. Each data point represents 2 biological replicates. Mean ± SD are shown.

(B) Schematic of flow cytometry data showing the expected results for each class of polarized, depolarized, permeable, and impermeable bacteria.

(C) Flow cytometry analysis of the membrane potential and permeability of *E. coli lptD4213* cells after 15 min incubation with 1% DMSO (solvent control), 5 μM CCCP, 25 μg/mL nisin (2× MIC), 0.8 μg/mL polymyxin B (2× MIC), 12.5 μg/mL SCH-79797 (2× MIC), or 2 μg/mL trimethoprim (10× MIC). The limits for the depolarized region were defined by comparing the values in the CCCP and solvent only controls. The limits for the permeabilized region were defined by comparing the nisin and solvent only controls.

SCH-79797 Treatment Can Kill Bacteria in Contexts Where Combination Therapy Fails

Having established that SCH-79797 disrupts both folate metabolism and membrane integrity, we sought to determine if these two targets can together explain how SCH-79797 kills bacteria. To address this question, we used BCP analysis to compare the cell morphology of bacteria treated with SCH-79797 to that of bacteria treated with a combination of two different antibiotics, one of which targets DHFR and one of which targets membrane integrity. Qualitative inspection suggested that SCH-79797-treated *E. coli* appeared similar to *E. coli lptD4213* cells treated with a combination of trimethoprim and nisin (Figure 6A). Quantification of the images confirmed that SCH-79797 clusters with the co-treatment of trimethoprim and nisin (Figure 6A). Co-treatment with polymyxin B and trimethoprim similarly clustered with SCH-79797, suggesting that this effect is due to membrane perturbation and not specific to the complex MoA of nisin (Hasper et al., 2006; Prince et al., 2016; Wiedemann et al., 2001)

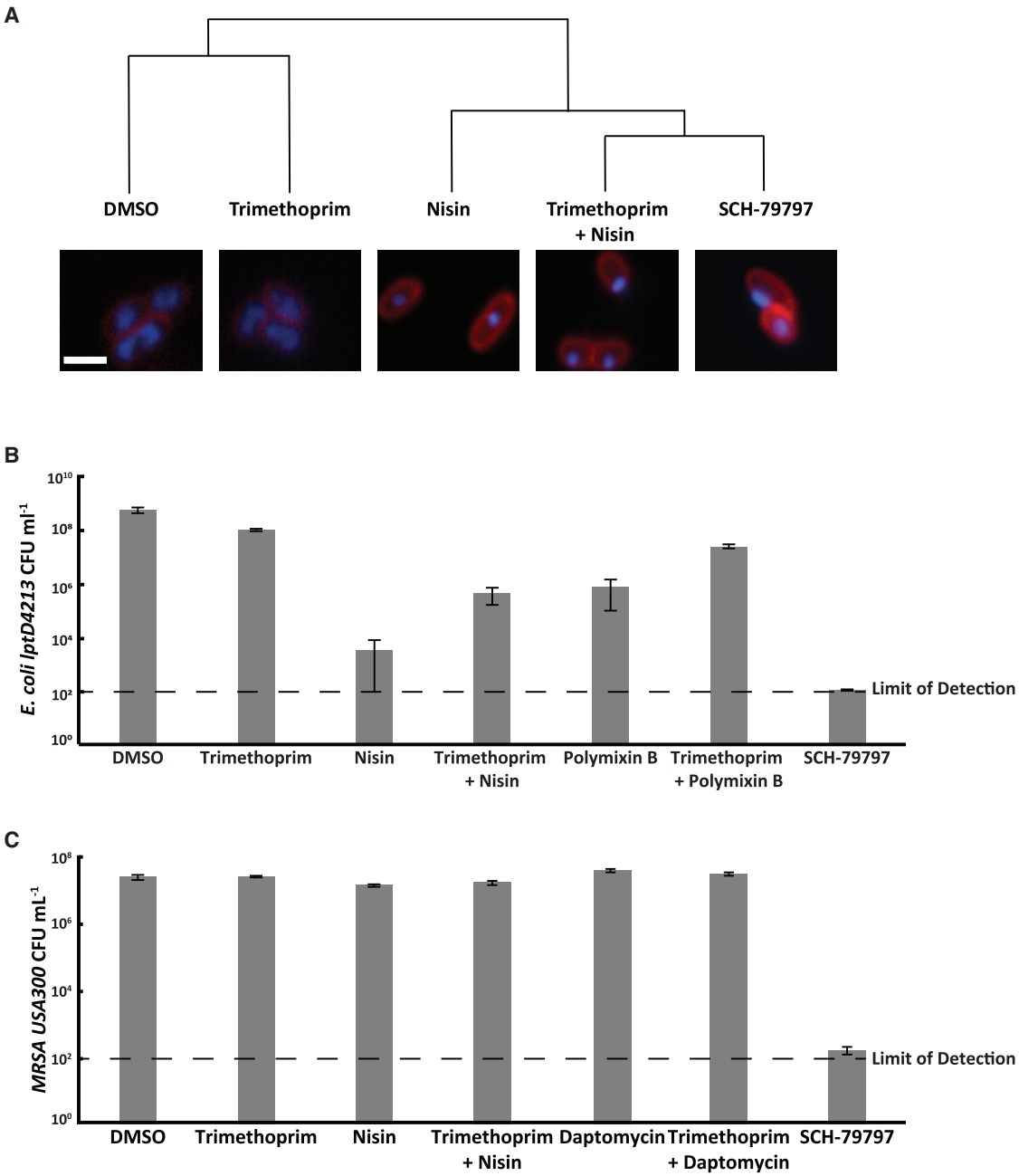

Figure 6. SCH-79797 Mimics Co-treatment with Folate Metabolism and Membrane Integrity Disruptors but Can Be More Effective Than Their Combination

(A) BCP analysis of *E. coli lptD4213* cells after 30 min of treatment with 1% DMSO, 6.3 μg/mL SCH-79797 (1× MIC), 2 μg/mL trimethoprim (10× MIC), 25 μg/mL nisin (2× MIC), or the combination of 2 μg/mL trimethoprim (10× MIC) and 25 μg/mL nisin (2× MIC). Cytological profiles were clustered by the first three principal components that account for at least 90% of the variance between samples. Cells were stained with DAPI, FM4-64, and SYTOX Green. Shown here are the merged images of DAPI (blue) and FM4-64 (red). Scale bar, 2 μm.

(B)The viability of *E. coli lptD4213* cells measured in CFU mL^{-1} after 2 h of treatment with 1% DMSO (solvent control), 2 μg/mL trimethoprim (10× MIC), 25 μg/mL nisin (2× MIC), the combination of 2 μg/mL trimethoprim (10× MIC) and 25 μg/mL nisin (2× MIC), 0.8 μg/mL polymixin B (2× MIC), the combination of 2 μg/mL trimethoprim (10× MIC) and 0.8 μg/mL polymixin B (2× MIC), or 3.1 μg/mL SCH-79797 (1× MIC). Each bar represents 3 biological replicates. Mean ± SD are shown.

(C) Viability of *S. aureus* MRSA USA300 persister cells measured in CFU mL^{-1} after 2 h of treatment with 1% DMSO (solvent control), 63 μg/mL trimethoprim (10× MIC), 100 μg/mL nisin (2× MIC), the combination of 63 μg/mL trimethoprim (10× MIC) and 50 μg/mL nisin (2× MIC), 63 μg/mL daptomycin (2× MIC), the combination of 63 μg/mL trimethoprim (10× MIC) and 63 μg/mL daptomycin (2× MIC), or 6.3 μg/mL SCH-79797 (1× MIC). Each bar represents 3 biological replicates. Mean ± SD are shown.

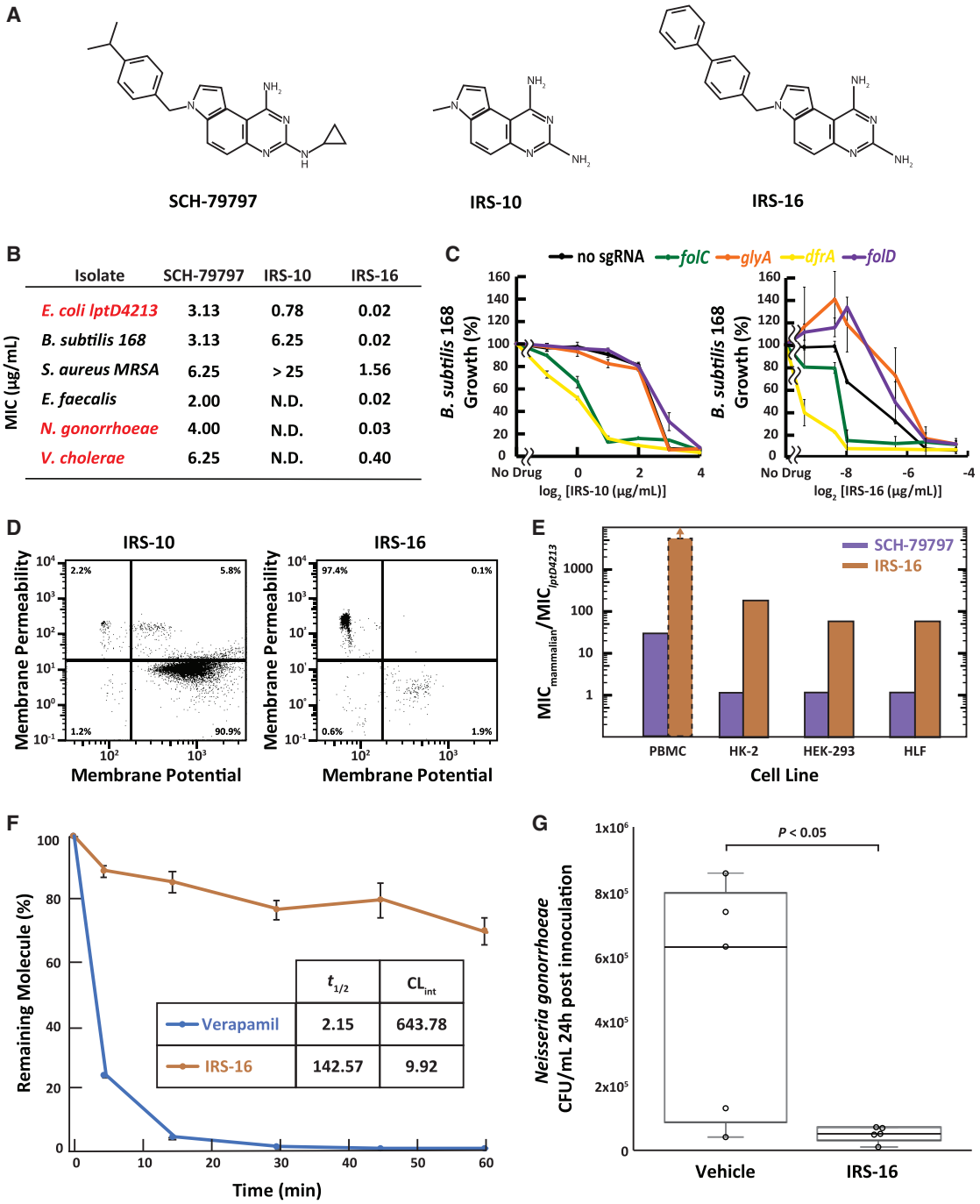

Figure 7. Derivates of SCH-79797 Show Increased Potency and the Ability to Help Clear Infection in Mouse Vaginal *N. gonorrhea* Model

(A) Structures of SCH-79797, the pyrroloquinazolinediamine core lacking the side chains (IRS-10), and the pyrroloquinazolinediamine core with a biphenyl decoration (IRS-16).

(B) The MICs of SCH-79797, IRS-10, and IRS-16 against a few selected species. For the MICs against additional strains, see Table S1.

(C) The growth of CRISPRi *B. subtilis* knockdown mutants involved in folate synthesis relative to a DMSO-treated control after treatment with IRS-10 or IRS-16. Bacterial growth was measured for 14 h and the final optical density (OD_{600}) of each condition was plotted against drug concentration. Each data point represents 2 biological replicates. Mean ± SD are shown.

(D) Flow cytometry analysis of the membrane potential and permeability of *E. coli lptD4213* cells after 15 min incubation with 0.4 μg/mL IRS-10 (1× MIC) or 0.02 μg/mL IRS-16 (1× MIC).

(E) Therapeutic index of SCH-79797 and IRS-16 was calculated by dividing the MIC of each drug for the indicated mammalian cell line by its MIC against *E. coli lptD4213*. The MIC of IRS-16 against PBMC was greater than the maximal drug concentrations tested.

(legend continued on next page)

(Figure S6). The fact that SCH-79797 clusters more closely to the co-treatments than to the individual treatments with trimethoprim or nisin/polymyxin B reinforces the conclusion that SCH-79797 kills bacteria by targeting both DHFR and the membrane. There are no other antibiotics that have been shown to target both folate metabolism and membrane integrity, indicating that SCH-79797 represents an antibiotic with a unique MoA. This result also explains why SCH-79797 failed to cluster with any of the known antibiotics in our BCP analysis (Figure 2B).

Combination antibiotic therapy has been suggested as a potential means of circumventing the rise of antibiotic resistance (Tamma et al., 2012; Tyers and Wright, 2019) but it has remained unclear whether it is better to combine multiple activities on the same molecule. To probe this issue, we measured the synergy of co-treatment with one antibiotic targeting dihydrofolate reductase and another targeting the membrane and compared their combined effectiveness to that of SCH-79797. Interestingly, when *E. coli lptD4213* cells were co-treated with trimethoprim and nisin, or co-treated with trimethoprim and polymixin B, the two antibiotics antagonized one another's activity, resulting in a greater number of viable cells remaining after 2 h of co-treatment (Figure 6B). MRSA USA300 persister cells (Kim et al., 2018) are resistant to treatment with the membrane-disrupting daptomycin (Chen et al., 2014; Taylor and Palmer, 2016). Treating MRSA USA300 persister cells with 63 μg/mL daptomycin (1× MIC) for 2 h did not reduce the number of CFUs remaining in the culture (Figure 6C). However, SCH-79797 treatment of MRSA robustly killed these persister cells while the combination of trimethoprim with either nisin or daptomycin could not (Figure 6C). These results suggest that the combination of two different antibacterial activities on the same molecular scaffold can, at least in the case of SCH-79797, produce a more potent antibacterial effect than co-treating with two antibiotics with the two separate targeting activities.

The Chemical Basis of the Two MoAs of SCH-79797

SCH-79797 consists of a pyrroloquinazolinediamine core that is substituted with an isopropylphenyl group on one side and a cyclopropyl moiety on the other. In order to test the function of the pyrroloquinazolinediamine core on the antibiotic activity of SCH-79797, we synthesized a derivative of SCH-79797 (Irresistin-10 or IRS-10) that lacks both side groups (Figure 7A). When compared to the parent molecule SCH-79797, removing the isopropylphenyl and cyclopropyl groups increased the potency against *E. coli lptD4213* but decreased the potency against *B. subtilis* 168, MRSA USA300, and *A. baumannii* AB17978 (Figure 7B; Table S1). To determine whether the pyrroloquinazolinediamine core of SCH-79797 is specifically involved in targeting folate metabolism or membrane integrity, we assessed the activity of IRS-10 using the *dfrA* and *folC* CRISPRi hypersensitivity assay and the quantitative flow cytometry membrane integrity assay. The CRISPRi hypersensitivity assay indicated that IRS-10 maintains the ability to inhibit folate metabolism, suggesting that the pyrroloquinazolinediamine core is sufficient to target DHFR (Figure 7C). However, unlike SCH-79797, $DiOC_2(3)$ and TO-PRO-3 staining showed that IRS-10 does not disrupt membrane polarity or permeability (Figure 7D). We also confirmed that IRS-10 directly inhibits the enzymatic activity of purified *E. coli* FolA (Figures 4D and 4E). IRS-10 proved to be a more potent inhibitor of FolA than SCH-79797 (IRS-10 IC_{50} = 65 ± 19 nM) (Figure 4D), suggesting that its increased efficacy against *E. coli* in cell culture can be explained by increased activity toward DHFR. Together, these findings suggest that the pyrroloquinazolinediamine core of SCH-79797 targets DHFR.

We next sought to determine if the isopropylbenzene side group is responsible for the membrane-targeting properties of SCH-79797. We thus obtained isopropylbenzene alone (also known as cumene) (Figure S7A) and determined its effects on membrane integrity and folate biosynthesis. $DiOC_2(3)$ and TO-PRO-3 staining showed that ispropylbenzene disrupts both membrane polarity and permeability (Figure S7B). Meanwhile, reduction of *dfrA* or *folC* levels by CRISPRi had no effect on the sensitivity of bacteria to isopropylbenzene (Figure S7C). These results support the conclusion that SCH-79797 is a dual-targeting compound where the pyrroloquinazolinediamine core specifically targets folate metabolism while the isopropylbenzene group specifically targets membrane integrity.

As a further test of whether the hydrophobic isopropylbenzene chain functions to target the membrane, we generated another small molecule, Irresistin-16 (IRS-16), in which we decorated the pyrroloquinazolinediamine core with a biphenyl group that is even more hydrophobic than isopropylbenzene (Figure 7A). As predicted from the inclusion of both folate-targeting and membrane-targeting moieties, *dfrA* and *folC* CRISPRi mutants proved hypersensitive to IRS-16 and IRS-16 disrupted membrane permeability and polarity by $DiOC_2(3)$ and TO-PRO-3 staining (Figures 7C and 7D). IRS-16 also had more potent antibiotic activity than IRS-10 against most bacteria tested (Figure 7B; Table S1), suggesting that targeting both membrane integrity and folate biosynthesis is more powerful than targeting folate metabolism alone.

The SCH-79797 Derivative IRS-16 Is Efficacious in a Mouse Infection Model

An effective antibiotic needs to be able to target pathogenic bacteria without killing mammalian hosts. To determine the concentrations required to inhibit the growth of mammalian cells, we treated several mammalian cell lines with both SCH-79797 and IRS-16, the derivative with the most potent antibiotic activity. SCH-79797 showed promising results with PBMC cells, as they required more than 10-fold higher doses for growth inhibition than those required for killing *E. coli lptD4213* (Figure 7E). However, SCH-79797 inhibited the growth of other mammalian cell lines, including HK-2, HEK293, and HLF, at doses comparable to the doses needed to kill bacteria. In contrast, IRS-16 killed bacteria at ~100–1,000-fold lower doses than those required to

(F) The stability of IRS-16 was measured following incubation with mouse liver microsomes. Each data point represents 2 biological replicates. Mean ± SD are shown.

(G) Treatment of mice with IRS-16 (10 mg/kg, i.v., twice a day [b.i.d.]) reduces the vaginal burden of *N. gonorrhoeae* 24 h after inoculation. p value from one-factor ANOVA.

affect mammalian cells in all cell lines tested (Figure 7E). In light of this larger therapeutic window, we focused our further *in vivo* analysis efforts on IRS-16.

Because IRS-16 preferentially killed bacteria in culture models, we proceeded to characterize its *in vivo* effects on mice. We determined the maximal tolerated dose (MTD) of IRS-16 to be 15 mg/kg when administered intravenously. A pharmacokinetic analysis revealed that at this MTD, the plasma concentration of IRS-16 peaked at 1.4 μg/mL with a half-life of 15.8 h (Figures S7D and S7E). Consistent with this robust *in vivo* stability, a mouse liver microsome study showed that IRS-16 is extremely stable as compared to a control drug, verapamil (Figure 7F).

Finally, we determined whether IRS-16 has antibiotic activity in a mouse bacterial infection model. For this purpose, we focused on *N. gonorrhoeae* as it is a Gram-negative pathogen for which there is an acute need for new antibiotics due to widespread resistance toward existing drugs (CDC, 2019). There is also a well-validated mouse vaginal infection model for *N. gonorrhoeae* (Jerse et al., 2002; Song et al., 2008). In bacterial culture, IRS-16 showed robust activity toward *N. gonorrhoeae*, with an MIC of 0.03 μg/mL (Table S1). Our pharmacokinetic analysis indicated that IRS-16 should persist in mice at concentrations above this MIC for nearly 48 h (Figures S7D and S7E). To test its *in vivo* efficacy, we inoculated the vaginal tracts of BALB/c mice with 1.85×10^6 CFU/mouse of *N. gonorrhoeae* ATCC 700825, treated with intravenous (i.v.) doses of either 10 mg/kg IRS-16 or vehicle control at 2 and 14 h post-infection, and assayed vaginal *N. gonorrhoeae* CFUs at 26 h post-infection. IRS-16 significantly reduced the vaginal load of *N. gonorrhoeae* ($p < 0.05$) as compared to the vehicle control (Figure 7G). Consistent with its favorable therapeutic index and pharmacokinetic profile, this result confirms that IRS-16 can function as an effective antibiotic in an *in vivo* mouse gonorrhea infection model.

DISCUSSION

Due to the rise in resistance to known antibiotics, there is an acute need for new antibiotics with the key features of having unique MoAs, potency toward Gram-negatives, and reduced susceptibility to resistance. Here, we describe a promising compound, SCH-79797, and its derivative, IRS-16, that are effective in animals and address these key criteria with a unique dual-targeting MoA, the ability to kill both Gram-negative and Gram-positive pathogens, and an undetectably low frequency of resistance. We also describe a systems-level pipeline that combines independent orthogonal approaches to characterize the MoA of SCH-79797 in the absence of resistant mutants. Specifically, we used BCP classification to categorize the MoA of SCH-79797 as distinct from those of 37 known antibiotics (Figure 2B). We then used thermal proteome profiling to identify DHFR as a candidate binding partner of SCH-79797 and confirmed that SCH-79797 inhibits folate metabolism through metabolomic analysis and CRISPRi genetic hypersensitivity (Figures 3B, 4B, and 4C). We confirmed that SCH-79797 directly inhibits DHFR activity by acting competitively toward its DHF substrate (Figures 4D and 4E). The BCP images also alerted us to a second potential target for SCH-79797, the bacterial membrane. Quantitative flow cytometry with dyes that report on membrane permeability and polarity confirmed that SCH-79797 has a folate-independent effect on bacterial membrane integrity (Figure 5C). Together, these assays constitute a pipeline that can be used in the future to rapidly characterize antibiotic MoAs *de novo*. Such a pipeline is especially important for compounds such as SCH-79797 that are not prone to resistance and do not mimic known MoAs. BCP, thermal proteome profiling, metabolomics, CRISPRi sensitivity, and flow cytometry are all assays that can be performed in small volumes, such that they can be readily scaled without the need for synthesizing large amounts of the compound in question. The orthogonal nature of the assays enables the independent identification of multiple MoAs, which may help in the discovery of unique antibiotic classes.

Both of the targets of SCH-79797 are relevant for its function as an antibiotic. The CRISPRi and metabolomic studies demonstrate that SCH-79797 actively disrupts folate metabolism in multiple bacterial species in a manner that is rate-limiting for growth (Figures 4B and 4C). Meanwhile, the flow cytometry assay demonstrates that SCH-79797 simultaneously disrupts membrane integrity even though folate inhibition itself has no effect on the membrane (Figure 5C). The ability of SCH-79797 to disrupt membrane integrity is particularly interesting given that membrane-disruptors are often selective for either Gram-positive or Gram-negative bacteria (Ling et al., 2015; Taylor and Palmer, 2016; Warren et al., 1957), while SCH-79797 proved potent against both Gram-positive pathogens like *S. aureus* and *E. faecalis* as well as Gram-negative pathogens like *A. baumannii*, *N. gonorrhoeae*, and pathogenic *E. coli* (Figure 1A). Host toxicity is often a concern for membrane-targeting antibiotics, and while SCH-79797 was well tolerated by some animal cells like *G. mellonella* wax worms and PBMC cells, it killed other mammalian cell lines at doses similar to those at which it functions as an antibiotic. Meanwhile, IRS-16, a derivative of SCH-79797, increased antibiotic activity without increasing mammalian toxicity, thereby increasing its therapeutic window >100-fold. The ability of IRS-16 to selectively target bacteria is consistent with a recent study of retinoid derivatives that provided proof-of-principle that small molecules can preferentially target bacterial membranes (Kim et al., 2018). Future biophysical characterization and medicinal chemistry will help to further increase potency and reduce toxicity.

The undetectably low frequency of resistance to SCH-79797 could result from its two distinct targets. Specifically, we were successful in isolating resistance mutants for mimics of each of its two individual targets, trimethoprim and nisin, but not for SCH-79797 (Figure 1E). The average mutation rate in *E. coli* is 2.1×10^{-7} per gene per generation (Chen and Zhang, 2013). If *E. coli* required 2 mutations to acquire resistance to SCH-79797, the number of bacteria that would be necessary to find a resistant mutant would be in the range of 10^{14}. Even if that represents an overestimate, humans are estimated to carry roughly 4×10^{13} bacteria in total, so such low frequencies of resistance would be unlikely to result in resistant mutants in a clinical context.

Our studies suggest that SCH-79797 is more potent than combination treatment with antibiotics that mimic its two activities, the DHFR-inhibitor trimethoprim and the membrane-disruptor nisin. Similarly, co-treatment with trimethoprim and polymyxin B showed antagonistic interactions (Figure 6B), while MRSA persister cells were killed by SCH-79797 but not by combined treatment with trimethoprim and daptomycin (Figure 6C). A potential explanation for the potency of SCH-79797 is that recruiting a DHFR inhibitor to the membrane could increase its effective concentration or potentiate its inactivation of DHFR by sequestering it. Permeabilizing the membrane could also enhance the access of SCH-79797 to its cytoplasmic DHFR target. The difference between SCH-79797 and the combination treatments could also be based on non-primary target effects such as differences in localized synergistic drug concentrations, drug uptake or efflux. Membrane-targeting molecules can act either synergistically or antagonistically with antibiotics with different MoAs (Brochado et al., 2018). Because trimethoprim and various membrane disruptors antagonize each other separately, but DHFR inhibition and membrane disruption synergize in the context of SCH-79797, combining antibiotic activities onto the same molecule could present a solution for bypassing this antagonistic effect. In any event, our results suggest that despite the promise of combination antibiotic therapies (Brochado et al., 2018; Tyers and Wright, 2019), an even more powerful approach could be to combine different targeting moieties onto the same chemical scaffold.

Discovering the MoA of SCH-79797 also enabled us to design derivatives that improve its efficacy. Our most promising derivative currently is IRS-16, in which we replaced the isopropylphenyl group with a biphenyl group (with the idea to increase the membrane-targeting activity) and removed the cyclopropyl side chain (to enhance the DHFR inhibition). IRS-16 showed improved ability to kill bacteria, with significantly lower MICs than SCH-79797. More importantly, IRS-16 did not similarly enhance the growth inhibition of mammalian cells. Thus, IRS-16 exhibited a promising therapeutic index, as reducing the concentration necessary to kill bacteria without affecting the concentration necessary to kill mammalian cells resulted in a compound that is >100-fold more potent toward bacteria than hosts. IRS-16 was also stable in mice and tolerated at doses significantly above the MIC for several hours. Finally, we confirmed that IRS-16 significantly reduced the burden of *N. gonorrhoeae* in a mouse vaginal infection model. *N. gonorrhoeae* is a Gram-negative pathogen with some of the highest rates of drug resistance for any pathogen. The acute need for new antibiotics to treat *N. gonorrhoeae* makes IRS-16 a particularly promising small molecule candidate for future development.

STAR★METHODS

Detailed methods are provided in the online version of this paper and include the following:

SUPPLEMENTAL INFORMATION

Supplemental Information can be found online at https://doi.org/10.1016/j.cell.2020.05.005.

ACKNOWLEDGMENTS

The *B. subtilis* CRISPR knockdown library was a kind gift from Jason M. Peters. Flow cytometry was performed in collaboration with Christina DeCoste (Princeton University Flow Cytometry Resource Facility [FCRF]). We appreciate the support and feedback from lab members in the Gitai and Shaevitz labs. Funding was provided in part by NIH (DP1AI124669 to Z.G., J.P.S., B.P.B., and J.K.M. and T32 GM007388 to J.K.M. and G.M.M.), as well as Princeton DFR Innovation Funds for New Ideas in Science (to J.K.M. and J.P.S.). Additional funding provided by the National Science Foundation (NSF PHY-1734030 to B.P.B.) and for the FCRF by the National Cancer Institute (NCI-CCSG P30CA072720-5921). The opinions, findings, and conclusions or recommendations expressed in this material contents are solely the responsibility of the authors and do not necessarily represent the official views of the NIH or the National Science Foundation.

AUTHOR CONTRIBUTIONS

Conceptualization, Z.G., J.K.M., M.Z.W., and H.K.; Methodology, Z.G., B.P.B., M.Z.W., A.M., A.T., M.M.S., J.R., S.H.-J.L., and H.K.; Software, M.Z.W., J.K.M., B.P.B., A.T., and M.M.S.; Validation, J.P.S.; Formal Analysis, B.P.B. and G.M.M.; Investigation, M.Z.W., J.K.M., J.P.S., G.M.M., A.M., A.T., M.M.S., S.H.-J.L., and B.P.B.; Resources, J.P.S. and M.Z.W.; Writing – Original Draft, Z.G. and J.K.M.; Writing – Reviewing & Editing, Z.G., B.P.B.,

J.P.S., H.K., and C.D.; Visualization, J.P.S., J.K.M., and B.P.B.; Supervision, Z.G., H.K., J.R., A.T., and M.M.S.; Funding Acquisition, Z.G., J.R., A.T., and M.M.S.

DECLARATION OF INTERESTS

A patent application describing the use of SCH-79797 as an antibiotic, as well as the pharmaceutical composition and use as antibiotic of derivatives is currently pending.

Received: June 6, 2019
Revised: February 24, 2020
Accepted: May 1, 2020
Published: June 3, 2020

REFERENCES

Ahn, H.S., Foster, C., Boykow, G., Stamford, A., Manna, M., and Graziano, M. (2000). Inhibition of cellular action of thrombin by N3-cyclopropyl-7-[[4-(1-methylethyl)phenyl]methyl]-7H-pyrrolo[3, 2-f]quinazoline-1,3-diamine (SCH 79797), a nonpeptide thrombin receptor antagonist. Biochem. Pharmacol. *60*, 1425–1434.

Amyes, S.G., and Smith, J.T. (1975). Thymineless mutants and their resistance to trimethoprim. J. Antimicrob. Chemother. *1*, 85–89.

Becher, I., Werner, T., Doce, C., Zaal, E.A., Tögel, I., Khan, C.A., Rueger, A., Muelbaier, M., Salzer, E., Berkers, C.R., et al. (2016). Thermal profiling reveals phenylalanine hydroxylase as an off-target of panobinostat. Nat. Chem. Biol. *12*, 908–910.

Bell-Pedersen, D., Galloway Salvo, J.L., and Belfort, M. (1991). A transcription terminator in the thymidylate synthase (thyA) structural gene of Escherichia coli and construction of a viable thyA:Kmr deletion. J. Bacteriol. *173*, 1193–1200.

Boucher, H.W., Talbot, G.H., Bradley, J.S., Edwards, J.E., Gilbert, D., Rice, L.B., Scheld, M., Spellberg, B., and Bartlett, J. (2009). Bad bugs, no drugs: no ESKAPE! An update from the Infectious Diseases Society of America. Clin. Infect. Dis. *48*, 1–12.

Brochado, A.R., Telzerow, A., Bobonis, J., Banzhaf, M., Mateus, A., Selkrig, J., Huth, E., Bassler, S., Zamarreño Beas, J., Zietek, M., et al. (2018). Species-specific activity of antibacterial drug combinations. Nature *559*, 259–263.

Butler, M.S., Blaskovich, M.A., and Cooper, M.A. (2017). Antibiotics in the clinical pipeline at the end of 2015. J. Antibiot. (Tokyo) *70*, 3–24.

Cammarata, M., Thyer, R., Lombardo, M., Anderson, A., Wright, D., Ellington, A., and Brodbelt, J.S. (2017). Characterization of trimethoprim resistant *E. coli* dihydrofolate reductase mutants by mass spectrometry and inhibition by propargyl-linked antifolates. Chem. Sci. (Camb.) *8*, 4062–4072.

CDC (2019). Antibiotic Resistance Threats in the United States (U.S. Department of Health and Human Services).

Chen, X., and Zhang, J. (2013). No gene-specific optimization of mutation rate in Escherichia coli. Mol. Biol. Evol. *30*, 1559–1562.

Chen, Y.F., Sun, T.L., Sun, Y., and Huang, H.W. (2014). Interaction of daptomycin with lipid bilayers: a lipid extracting effect. Biochemistry *53*, 5384–5392.

Chen, L., Ducker, G.S., Lu, W., Teng, X., and Rabinowitz, J.D. (2017). An LC-MS chemical derivatization method for the measurement of five different one-carbon states of cellular tetrahydrofolate. Anal. Bioanal. Chem. *409*, 5955–5964.

Coates, A.R., Halls, G., and Hu, Y. (2011). Novel classes of antibiotics or more of the same? Br. J. Pharmacol. *163*, 184–194.

Culyba, M.J., Mo, C.Y., and Kohli, R.M. (2015). Targets for Combating the Evolution of Acquired Antibiotic Resistance. Biochemistry *54*, 3573–3582.

Davies, J. (2006). Where have All the Antibiotics Gone? Can. J. Infect. Dis. Med. Microbiol. *17*, 287–290.

Gebhardt, M.J., Gallagher, L.A., Jacobson, R.K., Usacheva, E.A., Peterson, L.R., Zurawski, D.V., and Shuman, H.A. (2015). Joint Transcriptional Control of Virulence and Resistance to Antibiotic and Environmental Stress in Acinetobacter baumannii. MBio *6*, e01660-15.

Gleckman, R., Blagg, N., and Joubert, D.W. (1981). Trimethoprim: mechanisms of action, antimicrobial activity, bacterial resistance, pharmacokinetics, adverse reactions, and therapeutic indications. Pharmacotherapy *1*, 14–20.

Gobbetti, T., Cenac, N., Motta, J.-P., Rolland, C., Martin, L., Andrade-Gordon, P., Steinhoff, M., Barocelli, E., and Vergnolle, N. (2012). Serine protease inhibition reduces post-ischemic granulocyte recruitment in mouse intestine. Am. J. Pathol. *180*, 141–152.

Gupta, N., Liu, R., Shin, S., Sinha, R., Pogliano, J., Pogliano, K., Griffin, J.H., Nizet, V., and Corriden, R. (2018). SCH79797 improves outcomes in experimental bacterial pneumonia by boosting neutrophil killing and direct antibiotic activity. J. Antimicrob. Chemother. *73*, 1586–1594.

Gutnick, D., Calvo, J.M., Klopotowski, T., and Ames, B.N. (1969). Compounds which serve as the sole source of carbon or nitrogen for Salmonella typhimurium LT-2. J. Bacteriol. *100*, 215–219.

Hasper, H.E., Kramer, N.E., Smith, J.L., Hillman, J.D., Zachariah, C., Kuipers, O.P., de Kruijff, B., and Breukink, E. (2006). An alternative bactericidal mechanism of action for lantibiotic peptides that target lipid II. Science *313*, 1636–1637.

Hofer, U. (2019). The cost of antimicrobial resistance. Nat. Rev. Microbiol. *17*, 3.

Imai, Y., Meyer, K.J., Iinishi, A., Favre-Godal, Q., Green, R., Manuse, S., Caboni, M., Mori, M., Niles, S., Ghiglieri, M., et al. (2019). A new antibiotic selectively kills Gram-negative pathogens. Nature *576*, 459–464.

Jerse, A.E., Crow, E.T., Bordner, A.N., Rahman, I., Cornelissen, C.N., Moench, T.R., and Mehrazar, K. (2002). Growth of Neisseria gonorrhoeae in the female mouse genital tract does not require the gonococcal transferrin or hemoglobin receptors and may be enhanced by commensal lactobacilli. Infect. Immun. *70*, 2549–2558.

Karlowsky, J.A., Draghi, D.C., Jones, M.E., Thornsberry, C., Friedland, I.R., and Sahm, D.F. (2003). Surveillance for antimicrobial susceptibility among clinical isolates of Pseudomonas aeruginosa and Acinetobacter baumannii from hospitalized patients in the United States, 1998 to 2001. Antimicrob. Agents Chemother. *47*, 1681–1688.

Kim, W., Zhu, W., Hendricks, G.L., Van Tyne, D., Steele, A.D., Keohane, C.E., Fricke, N., Conery, A.L., Shen, S., Pan, W., et al. (2018). A new class of synthetic retinoid antibiotics effective against bacterial persisters. Nature *556*, 103–107.

King, A.C., and Wu, L. (2009). Macromolecular synthesis and membrane perturbation assays for mechanisms of action studies of antimicrobial agents. Curr. Protoc. Pharmacol. *Chapter 13*, Unit 13A.17.

Kwon, Y.K., Lu, W., Melamud, E., Khanam, N., Bognar, A., and Rabinowitz, J.D. (2008). A domino effect in antifolate drug action in Escherichia coli. Nat. Chem. Biol. *4*, 602–608.

Kwon, Y.K., Higgins, M.B., and Rabinowitz, J.D. (2010). Antifolate-induced depletion of intracellular glycine and purines inhibits thymineless death in E. coli. ACS Chem. Biol. *5*, 787–795.

Ling, L.L., Schneider, T., Peoples, A.J., and Spoering, A.L. (2015). A new antibiotic kills pathogens without detectable resistance. Nature *517*, 455–459.

Mateus, A., Bobonis, J., Kurzawa, N., Stein, F., Helm, D., Hevler, J., Typas, A., and Savitski, M.M. (2018). Thermal proteome profiling in bacteria: probing protein state *in vivo*. Mol. Syst. Biol. *14*, e8242.

McInnes, L., Healy, J., and Melville, J. (2018). UMAP: Uniform Manifold Approximation and Projection for Dimension Reduction. arXiv, arXiv:1802.03426.

McKeage, K. (2015). Finafloxacin: first global approval. Drugs *75*, 687–693.

Nonejuie, P., Burkart, M., Pogliano, K., and Pogliano, J. (2013). Bacterial cytological profiling rapidly identifies the cellular pathways targeted by antibacterial molecules. Proc. Natl. Acad. Sci. USA *110*, 16169–16174.

Novo, D., Perlmutter, N.G., Hunt, R.H., and Shapiro, H.M. (1999). Accurate flow cytometric membrane potential measurement in bacteria using diethyloxacarbocyanine and a ratiometric technique. Cytometry *35*, 55–63.

Novo, D.J., Perlmutter, N.G., Hunt, R.H., and Shapiro, H.M. (2000). Multiparameter flow cytometric analysis of antibiotic effects on membrane potential,

membrane permeability, and bacterial counts of Staphylococcus aureus and Micrococcus luteus. Antimicrob. Agents Chemother. *44*, 827–834.

O'Neill, J. (2014). AMR Review Paper–Tackling a Crisis for the Health and Wealth of Nations (AMR Review Paper).

Peleg, A.Y., Jara, S., Monga, D., Eliopoulos, G.M., Moellering, R.C., Jr., and Mylonakis, E. (2009). Galleria mellonella as a model system to study Acinetobacter baumannii pathogenesis and therapeutics. Antimicrob. Agents Chemother. *53*, 2605–2609.

Peters, J.M., Colavin, A., Shi, H., Czarny, T.L., Larson, M.H., Wong, S., Hawkins, J.S., Lu, C.H.S., Koo, B.-M.M., Marta, E., et al. (2016). A Comprehensive, CRISPR-based Functional Analysis of Essential Genes in Bacteria. Cell *165*, 1493–1506.

Prince, A., Sandhu, P., Ror, P., Dash, E., Sharma, S., Arakha, M., Jha, S., Akhter, Y., and Saleem, M. (2016). Lipid-II Independent Antimicrobial Mechanism of Nisin Depends On Its Crowding And Degree Of Oligomerization. Sci. Rep. *6*, 37908.

Randall, L.B., Georgi, E., Genzel, G.H., and Schweizer, H.P. (2016). Finafloxacin overcomes Burkholderia pseudomallei efflux-mediated fluoroquinolone resistance. J. Antimicrob. Chemother. *72*, 1258–1260.

Ruiz, N., Kahne, D., and Silhavy, T.J. (2006). Advances in understanding bacterial outer-membrane biogenesis. Nat. Rev. Microbiol. *4*, 57–66.

Savitski, M.M., Reinhard, F.B.M., Franken, H., Werner, T., Savitski, M.F., Eberhard, D., Martinez Molina, D., Jafari, R., Dovega, R.B., Klaeger, S., et al. (2014). Tracking cancer drugs in living cells by thermal profiling of the proteome. Science *346*, 1255784.

Song, W., Condron, S., Mocca, B.T., Veit, S.J., Hill, D., Abbas, A., and Jerse, A.E. (2008). Local and humoral immune responses against primary and repeat Neisseria gonorrhoeae genital tract infections of 17beta-estradiol-treated mice. Vaccine *26*, 5741–5751.

Soupene, E., van Heeswijk, W.C., Plumbridge, J., Stewart, V., Bertenthal, D., Lee, H., Prasad, G., Paliy, O., Charernnoppakul, P., and Kustu, S. (2003). Physiological studies of Escherichia coli strain MG1655: growth defects and apparent cross-regulation of gene expression. J. Bacteriol. *185*, 5611–5626.

Strande, J.L., Hsu, A., Su, J., Fu, X., Gross, G.J., and Baker, J.E. (2007). SCH 79797, a selective PAR1 antagonist, limits myocardial ischemia/reperfusion injury in rat hearts. Basic Res. Cardiol. *102*, 350–358.

Tamma, P.D., Cosgrove, S.E., and Maragakis, L.L. (2012). Combination therapy for treatment of infections with gram-negative bacteria. Clin. Microbiol. Rev. *25*, 450–470.

Taylor, S.D., and Palmer, M. (2016). The action mechanism of daptomycin. Bioorg. Med. Chem. *24*, 6253–6268.

Tenover, F.C., and Goering, R.V. (2009). Methicillin-resistant Staphylococcus aureus strain USA300: origin and epidemiology. J. Antimicrob. Chemother. *64*, 441–446.

Tyers, M., and Wright, G.D. (2019). Drug combinations: a strategy to extend the life of antibiotics in the 21st century. Nat. Rev. Microbiol. *17*, 141–155.

Ursell, T., Lee, T.K., Shiomi, D., Shi, H., Tropini, C., Monds, R.D., Colavin, A., Billings, G., Bhaya-Grossman, I., Broxton, M., et al. (2017). Rapid, precise quantification of bacterial cellular dimensions across a genomic-scale knockout library. BMC Biol. *15*, 17.

Viehman, J.A., Nguyen, M.H., and Doi, Y. (2014). Treatment options for carbapenem-resistant and extensively drug-resistant Acinetobacter baumannii infections. Drugs *74*, 1315–1333.

Warren, G.H., Gray, J., and Yurchenco, J.A. (1957). Effect of polymyxin on the lysis of Neisseria catarrhalis by lysozyme. J. Bacteriol. *74*, 788–793.

Werner, T., Sweetman, G., Savitski, M.F., Mathieson, T., Bantscheff, M., and Savitski, M.M. (2014). Ion coalescence of neutron encoded TMT 10-plex reporter ions. Anal. Chem. *86*, 3594–3601.

Wiedemann, I., Breukink, E., van Kraaij, C., Kuipers, O.P., Bierbaum, G., de Kruijff, B., and Sahl, H.-G. (2001). Specific binding of nisin to the peptidoglycan precursor lipid II combines pore formation and inhibition of cell wall biosynthesis for potent antibiotic activity. J. Biol. Chem. *276*, 1772–1779.

STAR★METHODS

KEY RESOURCES TABLE

REAGENT or RESOURCE	SOURCE	IDENTIFIER
Bacterial and Virus Strains		
E. coli lptD4213 ΔthyA	This paper	ZG1599
B. subtilis 168 CRISPRi Library	Jason Peters and Carol Gross	Peters et al., 2016
Detailed bacterial strain information, including strain identifiers, growth media and temperature, is provided in Table S1	N/A	N/A
Chemicals, Peptides, and Recombinant Proteins		
SCH-7979	Tocris Biosciences	1592
Ampicillin	MP Biomedicals	190148
Cumene	Sigma	PHR1210
Daptomycin	TCI	D4229
Gentamicin sulfate	Sigma	G1914
Meropenem trihydrate	TCI	M2279
Nisin	MP Biomedicals	155839
Novobiocin sodium salt	MP Biomedicals	0215595705
Polymyxin B sulfate salt	Sigma	P1004
Purified *E. coli* dihydrofolate reductase (FolA)	Genscript	N/A
DAPI	ThermoFisher	D1306
SYTOX Green Dead Cell Stain	ThermoFisher	S34860
FM4-64 Dye	ThermoFisher	T13320
Critical Commercial Assays		
BacLight Bacterial Membrane Potential kit	ThermoFisher	B34950
Colorimetric Dihydrofolate Reductase Assay Kit	Sigma	CS0340
Deposited Data		
Proteomics	ProteomeXchange Consortium	PXD013673
Flow cytometry	FlowRespository	FR-FCM-Z2JD
Raw images and Metabolomics Data	This Paper; DataSpace at Princeton University	N/A
Experimental Models: Cell Lines		
HEK293	ATCC	CRL-1573
HK2	ATCC	CRL-2190
HLF	Cell Applications	506K-05a
PBMC	TPCS	PB010C
Experimental Models: Organisms/Strains		
Male CD-1 mice	Pharmaron	N/A
Female ovariectomized BALB/c mice	Pharmacology Discovery Services Taiwan	N/A
Galleria mellonella	PetCo	2336624
Software and Algorithms		
MATLAB	MathWorks	https://www.mathworks.com/products/matlab.html
Fiji	Eliceiri/LOCI group at University of Washington	https://imagej.net/Fiji
R Studio	R Studio	https://rstudio.com/products/rstudio/

(*Continued on next page*)

Continued

REAGENT or RESOURCE	SOURCE	IDENTIFIER
FlowJo	FlowJo, LLC	https://www.flowjo.com/solutions/flowjo/downloads
Other		
Synergy HT microplate reader	BioTek	N/A
InfiniteM200 Pro microplate reader	Tecan	N/A
27G x 0.5 inch needle	BD Biosciences	305109
QuantaMaster 40 Spectrophotometer	HORIBA Instruments	N/A

RESOURCE AVAILABILITY

Lead Contact

Further information and requests for resources and reagents should be directed to and will be fulfilled by the Lead Contact, Zemer Gitai (zgitai@princeton.edu).

Materials Availability

The unique strain (*E. coli lptD4213 ΔthyA*) generated in this study are available from the Lead Contact.

Data and Code Availability

Other than specific datasets and analysis code listed below, the published article includes all datasets generated or analyzed during this study.

Bacterial Cytological Profiling Code

The BCP analysis code is available under a BSD 3-clause license at https://github.com/PrincetonUniversity/gitai-bacterialAutopsy and archived at https://doi.org/10.5281/zenodo.3758582.

Thermal Proteome Profiling Data

The mass spectrometry proteomics data have been deposited to the ProteomeXchange Consortium via the PRIDE partner repository with the dataset identifier PRIDE:PXD013673.

Flow Cytometry Data

Flow cytometry data has been deposited to FlowRepository with the dataset identifier FR-FCM-Z2JD https://flowrepository.org/id/FR-FCM-Z2JD.

Additional Raw Data

The raw microscopy images used for bacterial cytological profiling and raw metabolomics data are available at Princeton DataSpace https://dataspace.princeton.edu/jspui/handle/88435/dsp01cr56n3903.

EXPERIMENTAL MODEL AND SUBJECT DETAILS

Bacterial strains and growth conditions

Detailed bacterial strain information, including growth media and temperature, is provided in Table S1. Where listed, growth media were prepared according manufacturer recommendations: LB Broth and LB Broth supplemented with 0.3 mM thymine (BD Biosciences 244610, Alfa Aesar A15879), Brain Heart Infusion (BD Biosciences 237500), Tryptic Soy Broth (BD Biosciences 211825), Nutrient Broth (BD Biosciences 234000), and Gutnick Minimal Media (1.0 g/L K_2SO_4, 13.5 g/L K_2HPO_4, 4.7 g/L KH_2PO_4, 0.1 g/L of $MgSO_4$-$7H_2O$, 10 mM NH_4Cl as a nitrogen source, and 0.4% w/v glucose as a carbon source) (Gutnick et al., 1969), Terrific Broth (BD Biosciences 243820).

E. coli lptD4213 ΔthyA was constructed by moving *ΔthyA*::Km^r (Bell-Pedersen et al., 1991) into *E. coli lptD4213* by P1 transduction.

Mammalian cell lines

Detailed cell line information is provided in Table S1. Mammalian cell line toxicity assays were performed by Pharmaron, Inc. (Beijing, ROC).

Animal models

Pharmacokinetics determination

Care and handling of male CD-1 mice approximately 6-8 weeks old conformed to institutional animal care and use policies as carried out at Pharmaron, Inc. (Beijing, ROC).

Neisseria gonorrhoeae infection model

Care and handling of 5-week old ovariectomized BALB/c mice conformed to institutional animal care and use policies as carried out at Pharmacology Discovery Services Taiwan, Ltd. (New Taipei City, TW).

METHOD DETAILS

Minimum inhibitory concentration assays

The minimum inhibitory concentration (MIC) of each antibiotic was defined as the lowest concentration of antibiotic that resulted in no visible growth. MICs were measured by diluting overnight cultures 1:150 and then adding 2-fold dilutions of each antibiotic in 96-well plates and grown with shaking at 37°C. Cell growth was monitored by measuring the OD_{600}. Assays performed by Pharmacology Discovery Services (New Taipei City, TW) and Pharmaron Inc. (Beijing, ROC) are indicated in Table S1. For MIC measurements done in-house, OD_{600} readings were measured by either a BioTek Synergy HT (Winooski, VT) or Tecan InfiniteM200 Pro (Männedorf, CH) microplate reader. In locations where drug concentrations are listed, they are included both as a relative fold change compared to the MIC for that bacterial strain and drug combination (1X MIC, 2X MIC, etc) as well as an absolute concentration (1 μg/mL, 2 μg/mL, etc).

Compound library

Compounds were sourced from commercial vendors: MicrosourceDiversity, Aldrich, Selleckchem, Chiromics, and Chembridge. Each compound dissolved in DMSO at 50 μM and then was screened for antibiotic activity against *E. coli lptD4213* growing in Terrific Broth. After normalizing for plate-to-plate variation, an OD_{600} of half the median plate OD_{600} was used as a cutoff, below which any compound was assumed to have inhibited the growth of *E. coli lptD4213* and above which compounds were assumed to be ineffective. Compounds that either had not been previously identified as antibiotics or had unknown or ambiguous mechanisms of action were chosen for further investigation and their MIC's were measured using the microdilution method described above.

Galleria mellonella killing assay

All *Galleria mellonella* larvae were obtained from Vita-Bugs©, distributed through PetCo© (2336624, San Diego, CA), and kept in a 20°C chamber. All injections were administered using a sterile 1 mL syringe with a 27G x 0.5 in needle (BD 305109) attached to a syringe pump (KD Scientific, 78-8210) delivered at a rate of 250 μL/min into the fourth leg of the worm. Prior to injection, the site was sterilized with ethanol. *A. baumannii* AB17978 (10^5 CFU/larva) and drug dissolved in DMSO (SCH-79797 at 66.6 μg/larva, gentamicin at 66.6 μg/larva, merapenem at 66.6 μg/larva) were pre-mixed prior to injection. The viability of each injected larva was determined by prodding each larva with a dowel and observing whether there was subsequent movement.

Colony forming units assay

Overnight *E. coli lptD4213* or *S. aureus* MRSA USA300 cultures were diluted 1:100 in fresh media and grown to mid exponential phase (OD_{600} = 0.4-0.6). Each culture was then diluted 1:10 into fresh media and then treated with the indicated concentration of each antibiotic. Each time point was taken by removing 150 μL and performing 10-fold serial dilutions. Six dilutions of each condition were then plated in the absence of antibiotic and grown at 37°C overnight. Colony forming units (CFU's) were measured by counting the resulting number of colonies the next day.

S. aureus MRSA persister cell assay

Stationary phase *S. aureus* cells have the same antibiotic tolerant properties of persister cells (Kim et al., 2018). Thus, overnight MRSA USA300 cultures were used to measure the effectiveness of SCH-79797 against persister cells. An overnight *S. aureus* MRSA USA300 culture was diluted 1:100 in PBS and then then treated with the indicated concentration of each antibiotic. After a 2 hour incubation with shaking at 37°C, 150 μL from each treatment condition was taken and 10-fold serial dilutions were performed. Six dilutions of each condition were then plated in the absence of antibiotic and grown at 37°C overnight. CFU's were measured by counting the resulting number of colonies the next day.

Serial passaging assay to evolve resistance

MICs of two biological replicates of *S. aureus MRSA* USA300 or *A. baumannii* AB17978 were obtained against the indicated antibiotics. Cells that grew in 0.5X MIC of the indicated antibiotics were subsequently cultured in the absence of antibiotics, and the MIC was then remeasured. This is a single passage and was repeated for 5-30 passages. Cells from each passage were stored as a frozen stock. Resistance was confirmed by comparing the MICs of resistant mutants against *S. aureus MRSA* USA300 or *A. baumannii* AB17978 that had not been previously exposed to the indicated antibiotics.

Bacterial cytological profiling

Compound library

Following the protocol of Nonejuie et al. (2013), overnight *E. coli lptD4213* cultures were diluted 1:100 in LB and grown at 30°C for 90 minutes on a roller drum. Each culture was then treated with 5X the MIC and incubated at 30°C with slight agitation. Following antibiotic treatment, cells were stained with 0.5 μM SYTOX Green, 1 μg/mL FM4-64, and 2 μg/mL DAPI for incubated for 10 minutes. Each stained culture was then centrifuged at 3220 r*cf.* for 40 s and resuspended in 1/10 volume of LB. Cells spotted onto a 1.2% agarose pad in 20% LB medium for imaging. Images were collected on a Nikon 90i upright microscope equipped with a 100X 1.4 N.A. objective (Nikon Instruments Inc., Melville, NY) and a RoleraXR (Photometrics, Tucson, AZ) camera. Microscope control and image acquisition were performed in NIS Elements.

Dual-treatment

In dual-treatment experiments (Figures 6A and S6), overnight *E. coli lptD4213* cultures were diluted 1:100 and grown to early-mid exponential phase (OD_{600} = 0.4-0.6). Each culture was then diluted 1:10 into fresh LB and treated with the desired concentration of antibiotic for 10 minutes. Following antibiotic treatment, cells were stained with 0.5 μM SYTOX Green, 1 μg/mL FM4-64, and 2 μg/mL DAPI. Each stained culture was then spotted onto a 1.5% agar pad supplemented with casamino acids and glucose in M63 (15 mM $(NH_4)_2SO_4$, 100 mM KH_2PO_4, 1.7 μM $FeSO_4$, 0.5% glucose, 0.2% casamino acids, 1 mM $MgSO_4$). Images were collected on either Nikon 90i upright microscope equipped with a 100X 1.4 N.A. objective (Nikon) or a Nikon Ti-E inverted microscope equipped with a 100X 1.4 NA objective. Both microscopes utilize an Orca Flash4 camera (Hamamatsu, Bridgewater, NJ). Microscope control and image acquisition were performed in NIS Elements (Nikon).

Image analysis

Following imaging, the *E. coli* cells were segmented (Ursell et al., 2017) and single-cell features were extracted using custom MATLAB code (Mathworks, Natwick, MA). Clustering was performed using the single-linkage method with MANOVA (Figure 2, MATLAB functions manova1, manovacluster). Before applying the UMAP dimensionality reduction technique (McInnes et al., 2018), each of the 14 cytological features was normalized into a z-score by subtracting off the mean and dividing by the standard deviation of that feature (Figure S2). Principal component analysis was performed using the prcomp function in R and clustering was performed using the single-linkage method (Figure 6).

Thermal proteome profiling

Thermal proteome profiling experiments were performed following Mateus et al. (2018). Whole cell samples were treated with 0.6, 1.1, 2.2, 4.4 μg/mL SCH-79797 or 0.1, 0.5, 2.3, 11.6 μg/mL trimethoprim. Cell lysate samples were treated with 0.4, 1.8, 8.9, 44.4 μg/mL SCH-79797 or 0.1, 0.5, 2.3, 11.6 μg/mL trimethoprim. After heat treatment, the soluble fraction was collected, digested with trypsin and peptides were labeled with tandem mass tags (Werner et al., 2014). Samples were subjected to two-dimensional liquid chromatography and analyzed on a Q Exactive Plus mass spectrometer (Thermo Fisher Scientific). While the data collected is proteome wide, three different cutoffs were used to define three classes of potential targets. The color of the point indicates the signal maximal effect size across all temperatures and the largest change in abundance across all concentrations was selected for continued analysis (Dots, Figure 3.) A mild effect indicates at least one temperature had a change in abundance of at least 25% in both whole cell and cell lysate treatments (Triangles, Figure 3) Proteins that had a change in abundance of at least 25% at three or more temperatures (Squares, Figure 3). To be considered a consistent effect, the change in abundance of the protein had to show the same sign at least 90% of the time and have an effect size of at least 1 (2-fold) in either whole cells or cell lysates.

Metabolomics

Overnight *E. coli* NCM3722 cultures were grown and diluted 1:100 in Gutnick Minimal Media and grown to early-mid exponential phase (OD_{600} = 0.4-0.6). Cultures were treated with either 13.9 μg/mL SCH-79797 (1X MIC) or 0.15 μg/mL trimethoprim (1X MIC) for 15 minutes. Folates were extracted by vacuum filtering 15 mL of treated cells using 0.45 μm HNWP Millipore nylon membranes and immediately placing filters into an ice-cold quenching solution containing 40:40:20 Methanol:acetonitrile:25 mM NH_4OAc + 0.1% sodium Ascorbic in HPLC grade water. The resulting solution was then centrifuged at 16,000 × g for 1.5 min at 4°C and the supernatant saved for mass spectrometry analysis. Mass spectrometry analysis was performed as described in Chen et al. (2017).

Dihydrofolate reductase activity assay

E. coli dihydrofolate reductase (FolA) was purified by Genscript (Piscataway, NJ). The enzymatic activity of FolA was measured using a colorimetric dihydrofolate reductase assay kit (Sigma CS0340) using a QuantaMaster 40 Spectrophotometer (Photon Technology International Inc., Edison, NJ). The kit measures FolA activity by monitoring the change in sample absorbance at 340 nm due to FolA-dependent NADPH consumption. For each condition, 1 μL purified enzyme in storage buffer (1X PBS, 10% glycerol, pH 7.4) was thawed on ice and added to 1000 μL 1X assay buffer immediately before assaying. After mixing the reaction components together, the 100 μL reaction volume was pipetted into a 1 mM pathlength quartz cuvette and the transmitted light intensity at 340 nm was measured for 100 s at 1 kHz sampling. These high frequency readings were downsampled by averaging to 1 Hz and the activity of each sample was calculated from the slope (β) a linear regression of the log transformed intensity measurements using MATLAB. Because the enzyme was only moderately stable in assay buffer (half-time ~20 minutes), all enzymatic measurements were

normalized to a standard condition (60 μM NADPH and 100 μM DHF) that was measured immediately before the sample of interest. The relative activity was calculated from $(\beta_{sample} - \beta_{noEnzyme})/(\beta_{standard} - \beta_{noEnzyme})$.

Membrane potential and permeability assay

Overnight *E. coli lptD4213* and *B. subtilis* 168 cultures were diluted 1:100 and grown to early-mid exponential phase (OD_{600} = 0.4-0.6) at 37°C. Each culture was then diluted 1:10 into PBS and treated with the desired concentration of antibiotic for 15 minutes. Cells were then stained with the BacLight Bacterial Membrane Potential kit (ThermoFisher B34950). This kit uses DiOC2(3) to measure a cell's membrane potential as a ratio of green (488 nm ex, 525/50 nm em) to red (488 nm ex, 610/20 nm em) (Novo et al., 1999). Membrane integrity was measured by staining cells with TO-PRO-3, a dye that is excluded from cells with an intact membrane (640 nm ex, 670/30 nm em). The LSRII flow cytometer (BD Biosciences) at the Flow Cytometry Resource Facility, Princeton University, was used to measure the fluorescent intensities of both dyes in response to antibiotic treatment. 100,000 events were recorded for each data file. Data was analyzed using FlowJo v10 software (FlowJo LLC, Ashland, OR).

Mammalian cell cytotoxicity

In a white, opaque, 384-well plate, either HEK293 (500 cells/well), HK-2 (500 cells/well), HLF cells (500 cells/well) or PBMC (3000 cells/well) cells were seeded overnight. After 24 hours, DMSO or compounds were added in 3-fold dilutions and incubated for 72 hours. CyQUANT Detection Reagent was added in equal volume and incubated for 1 hour. Fluorescence was read from the bottom of plate with standard green filter set (508/527 nm ex). Cell toxicity was evaluated by Pharmaron, Inc. (Beijing, ROC).

Mouse liver microsomal stability

The metabolic stability of IRS-16 was tested in mouse liver microsomes with NADPH and UDPGA over a period of 1 hour. IRS-16 (2 μM) and Verapamil (2 μM, positive control) were added to 0.5 mg/mL microsomes. Aliquots of 50 μL were taken from the reaction solution at 0.5, 5, 15, 30, 45 and 60 minutes. The reaction was stopped by the addition of 5 volumes of cold acetonitrile with IS (100 nM alprazolam, 200 nM caffeine, and 100 nM tolbutamide). Samples were centrifuged at 3,220xg for 40 minutes. Aliquots of 100 μL of the supernatant were mixed with 100 μL of ultra-pure H_2O and then used for LC-MS/MS analysis. Mouse liver microsomal stability was evaluated by Pharmaron, Inc. (Beijing, ROC).

Pharmacokinetic analysis

6-8 week old male CD-1 mice were injected intravenously with a single dose of IRS-16 at 15 mg/kg in 5% DMSO + 95% (20% HP-β-CD in water, W/V) and showed no adverse effects. Plasma measurements were averaged from 2 mice at the indicated time points following administration. Concentration was determined by LC/MS. Pharmacokinetic assay was performed by Pharmaron, Inc. (Beijing, ROC).

Neisseria gonorrhea vaginal infection model

Groups of 5 ovariectomized BALB/c mice 5 weeks of age were used. Animals were subcutaneously injected with a water soluble form of estradiol at 0.23 mg/mouse on day −2, 0, 2, 4 and 6.Starting from day −2, and following inoculation to the study end, mice were dosed twice daily with streptomycin (1.2 mg/mouse) and vancomycin (0.6 mg/mouse) by IP injection to minimize the vaginal flora. Trimethoprim sulfate (0.04 g/100 mL) was administered in drinking water. At day 0, mice were anesthetized by ketamine (100 mg/kg) and xylazine (10 mg/kg) through IP injection, and then inoculated intravaginally with 1.0-2.0 × 10^6 CFU of *N. gonorrhoeae* (FA1090, ATCC 700825). Before inoculation, the mouse vagina was first rinsed with 30 μL of 50 mM HEPES (pH 7.4) followed by inoculation with 20 μL gonococci suspension in PBS containing 0.5 mM $CaCl_2$ and 1 mM $MgCl_2$. IRS-16 or vehicle were administered 2 h and 12 h after inoculation. Mice are euthanized with CO_2 asphyxiation after 2 h and 24 h. Lavage was performed with 400 μL GC broth containing 0.05% saponin to recover vaginal bacteria. The bacterial suspensions were plated onto chocolate agar to determine the *N. gonorrhoeae* counts. *N. gonorrhoeae* vaginal infection model was performed by Pharmacology Discovery Services (New Taipei City, TW).

QUANTIFICATION AND STATISTICAL ANALYSIS

Center, spread, and statistical significance

For all assays except the *Neisseria gonorrhea* vaginal infection model, we use the arithmetic mean and standard deviation across multiple biological replicates as our measures of center and spread. The particular numbers of replicates for each experiment type are included in the respective figure legends. For the *Neisseria gonorrhea* vaginal infection model, we display median, Q1, Q3, and the values for each of the five individual mice in each sample cohort are (Figure 7G).

Statistical significance for *Galleria mellonella* killing assays were determined from Mantel-Cox test using Prism 8.1.2 (GraphPad, San Diego, CA). Each of three independent cohorts started with twelve animals. p values can be found in Table S2. For the *Neisseria gonorrhea* vaginal infection model, significance ($p < 0.05$) was determined from a one-factor ANOVA.

Bacterial cytological profiling

Hierarchical-clustering of the cytological features was performed using the single-linkage method with MANOVA (Figure 2, MATLAB functions manova1, manovacluster). Before applying the UMAP dimensionality reduction technique (McInnes et al., 2018), each of the 14 cytological features was normalized into a z-score by subtracting off the mean and dividing by the standard deviation of that feature (Figure S2). Principal component analysis was performed using the prcomp function in R and clustering was performed using the single-linkage method (Figure 6). Details of the dimensionality reduction technique and hierarchical clustering method are included in the respective figure legends.

Thermal proteome profiling

While the data collected is proteome wide, three different cutoffs were used to define three classes of potential targets. The color of the point indicates the signal maximal effect size across all temperatures (nTemp = 10) and the largest change in abundance across all concentrations (nConc = 4) was selected for continued analysis (Dots, Figure 3.) A mild effect indicates at least one temperature had a change in abundance of at least 25% in both whole cell and cell lysate treatments (Triangles, Figure 3) Proteins that had a change in abundance of at least 25% at three or more temperatures (Squares, Figure 3). To be considered a consistent effect, the change in abundance of the protein had to show the same sign at least 90% of the time and have an effect size of at least 1 (2-fold) in either whole cells or cell lysates. The details for these symbols and cutoffs are included in the respective figure legend.

Flow cytometry analysis

100,000 events were recorded for each flow cytometry sample and analyzed using FloJo v10. Gates used to quantify the fraction of events with depolarized or permeabilized membranes were determined from control samples treated with CCCP or nisin respectively. These details are included in the respective figure legends (Figures 5C, 7D, S5, and S7B).

Pharmacokinetic analysis

Plasma measurements were averaged from 2 mice at the indicated time points following administration. After the rapid initial approach to pseudoequilibrium, filled data symbols were used as the input for terminal half-life determination (Figure S7D). Pharmacokinetic parameters estimated of a non-compartmental model of IRS-16 serum levels (Figure S7D). These details are included in the respective figure legends.

Supplemental Figures

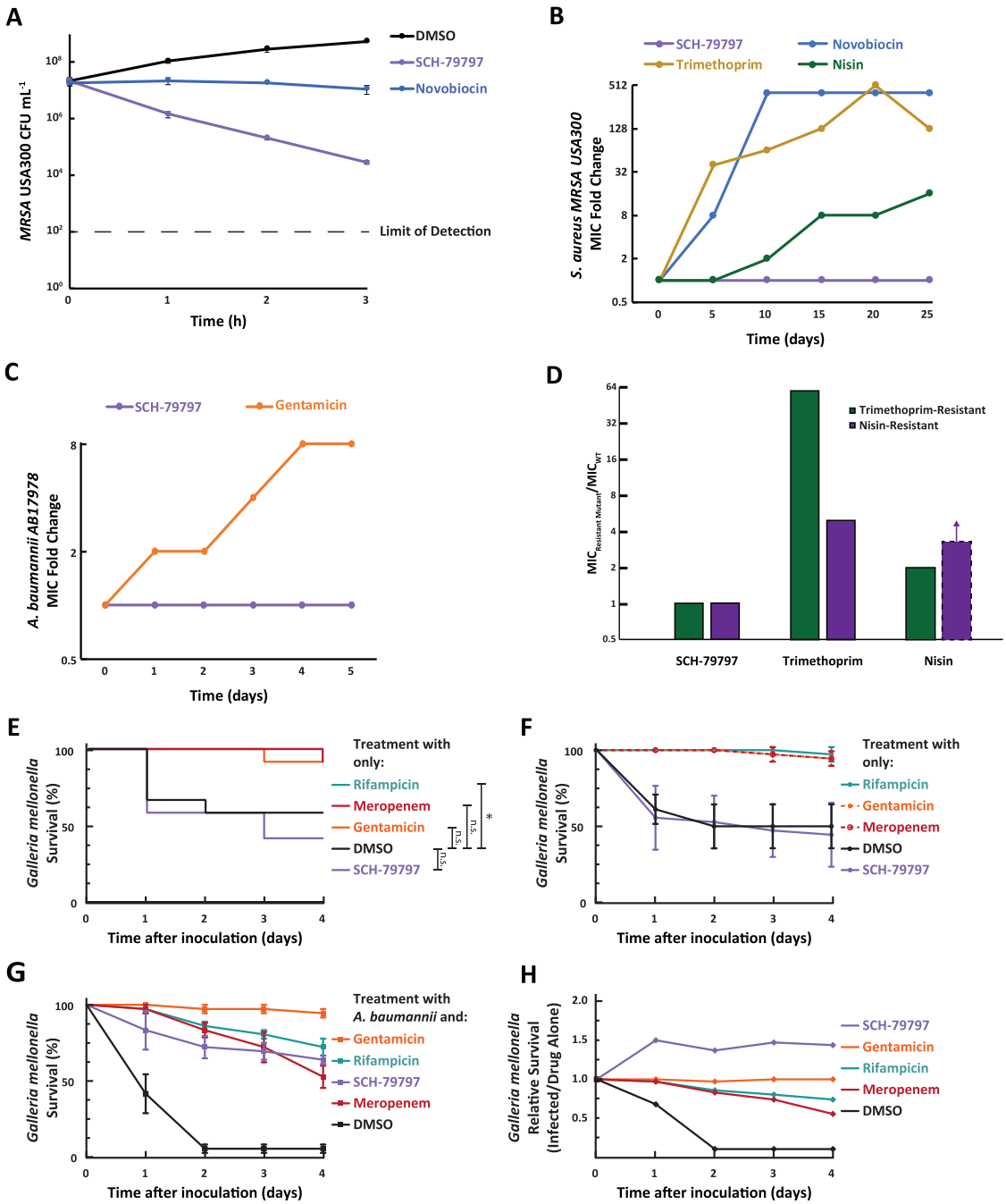

Figure S1. SCH-79797 Is Bactericidal against *Staphylococcus aureus*, Exhibits Undetectably Low Rates of Resistance, and Is an Effective Antibiotic in an Infection Model of *Galleria mellonella* by *Acinetobacter baumannii*, Related to Figure 1

A. Colony forming units (CFU mL^{-1}) after 3-hour treatment of *S. aureus* MRSA USA300 with solvent only (1% DMSO), and 6.3 μg/mL SCH-79797 (1X MIC), or 4.0 μg/mL novobiocin (5X MIC). Each data point represents 3 independent samples and 3 technical replicates. Mean ± SD are shown. B. Fold increase in resistance of *S. aureus* MRSA USA300 to SCH-79797, novobiocin, trimethoprim, or nisin after 25 days of serial passaging in each drug. C. Fold increase in resistance of *A. baumannii* AB17978 to SCH-79797 and gentamicin after 5 days of serial passaging in each drug. D. Fold increase in the susceptibility of *S. aureus* MRSA USA300 mutants to the indicated antibiotics. Trimethoprim and nisin resistant mutants were obtained from serial passaging in respective antibiotics. E-F. The percent survival of non-infected *G. mellonella* wax worms after treatment with 2 μL/larva of 100% DMSO, 67 μg/larva SCH-79797, 67 μg/larva gentamicin,

(legend continued on next page)

67 μg/larva rifampicin, or 67 μg/larva meropenem. Data in (E) represents a typical cohort (n = 12) from a biological triplicate and the pooled results are presented in (F). p values are determined from a Mantel-Cox test using Prism (n.s., $p \geq 0.05$; *$p < 0.05$). G. The percent survival of *G. mellonella* wax worms infected with *A. baumannii* (AB 17978) and concomitantly treated with 67 μg/larva SCH-79797, 67 μg/larva gentamicin, 67 μg/larva rifampicin, or 67 μg/larva meropenem. Data represents the pooled results from a biological triplicate. H. The relative survival of drug-treated of *G. mellonella* wax worms infected with *A. baumannii* (AB 17978) and treated concomitantly with antibiotics relative to larvae treated with antibiotics only without infection. Data represents the pooled results from a biological triplicate.

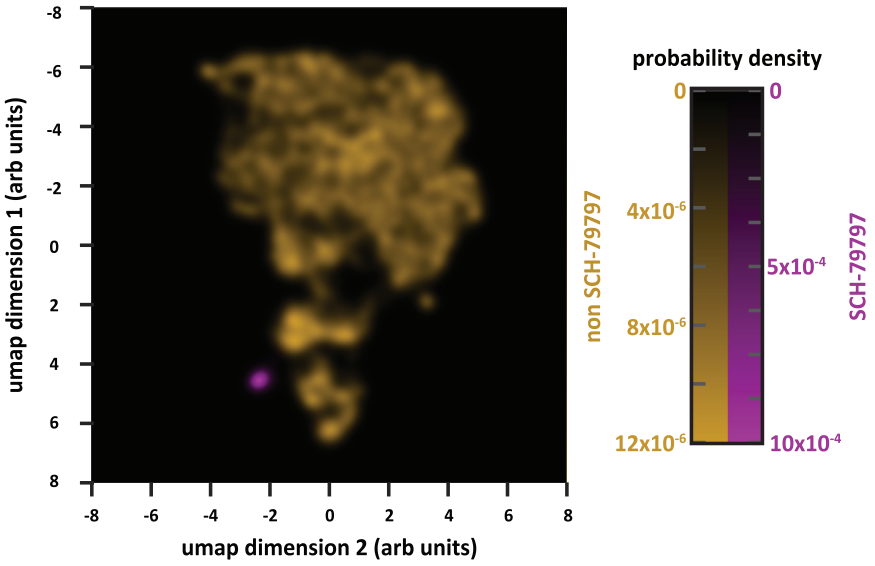

Figure S2. Bacterial Cytological Profiling of SCH-79797 and Antibiotics with Known Mechanisms of Action, Related to Figure 2

Dimensionality reduction of all treatments using umap were replotted using two color channels, one for only SCH-79797 treatments and one for the remaining conditions. Density smoothed with a σ = 0.1 width Gaussian kernel.

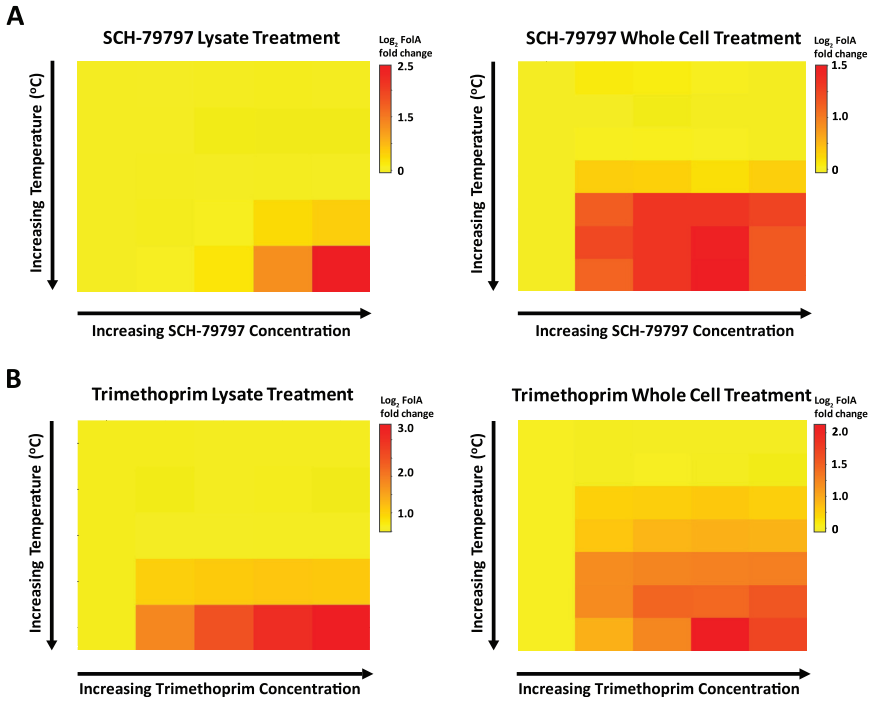

Figure S3. Thermal Stability of Dihydrofolate Reductase Increases after SCH-79797 and Trimethoprim Treatment, Related to Figure 3

A-B. The relative thermal stability of *E. coli* dihydrofolate reductase (FolA) after treatment of whole cell and cell lysate samples with (A) SCH-79797 and (B) trimethoprim. Changes in thermal stability were determined by measuring changes in the abundance of FolA across 10 different temperatures ranging from 42-72°C and 4 drug concentrations and a vehicle control.

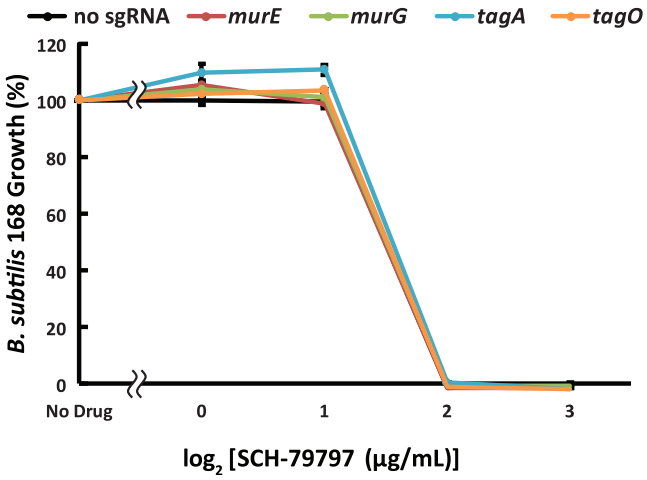

Figure S4. CRISPRi Mutants Not Involved in Folate Metabolism Are Not Sensitized to SCH-79797, Related to Figure 4

A. The growth of CRISPRi *B. subtilis* knockdown mutants relative to a DMSO-treated control after SCH-79797 treatment. Bacterial growth was measured for 14 h and the final optical density (OD_{600}) of each condition was plotted against drug concentration. Each data point represents 2 independent replicates. Mean ± SD are shown.

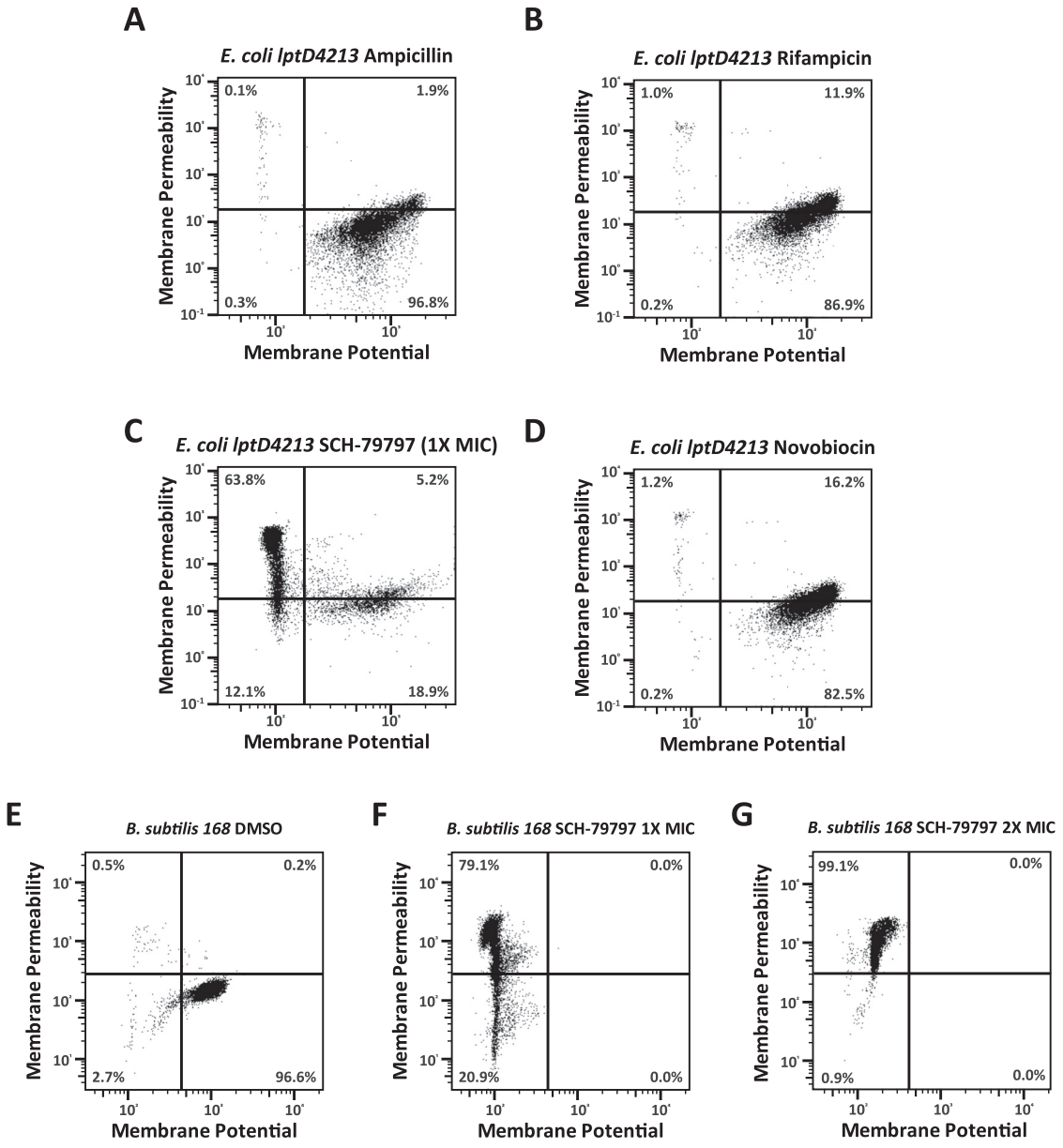

Figure S5. Treatment with Ampicillin, Rifampicin, and Novobiocin Does Not Disrupt Membrane Integrity while SCH-79797 Disrupts *Bacillus subtilis* 168 Membrane Integrity, Related to Figure 5

A-D. Flow cytometry analysis of the membrane potential and permeability of *E. coli lptD4213* cells after 15 minute incubation with (A) 0.06 μg/mL ampicillin (2X MIC), (B) 0.002 μg/mL rifampicin (2X MIC), (C) 3.1 μg/mL SCH-79797 (1X MIC), or (D) 0.12μg/mL novobiocin (2X MIC). The limits for the depolarized region were defined by comparing the values in the CCCP and solvent only controls. The limits for the permeabilized region were defined by comparing the nisin and solvent only controls. E-G. Flow cytometry analysis of the membrane potential and permeability of *B. subtilis* 168 cells after 15 minute incubation with (E) 1% DMSO, (F) 3.1 μg/mL SCH-79797 (1X MIC), or (G) 6.2 μg/mL SCH-79797 (2X MIC). The limits for the regions were defined from the solvent only controls.

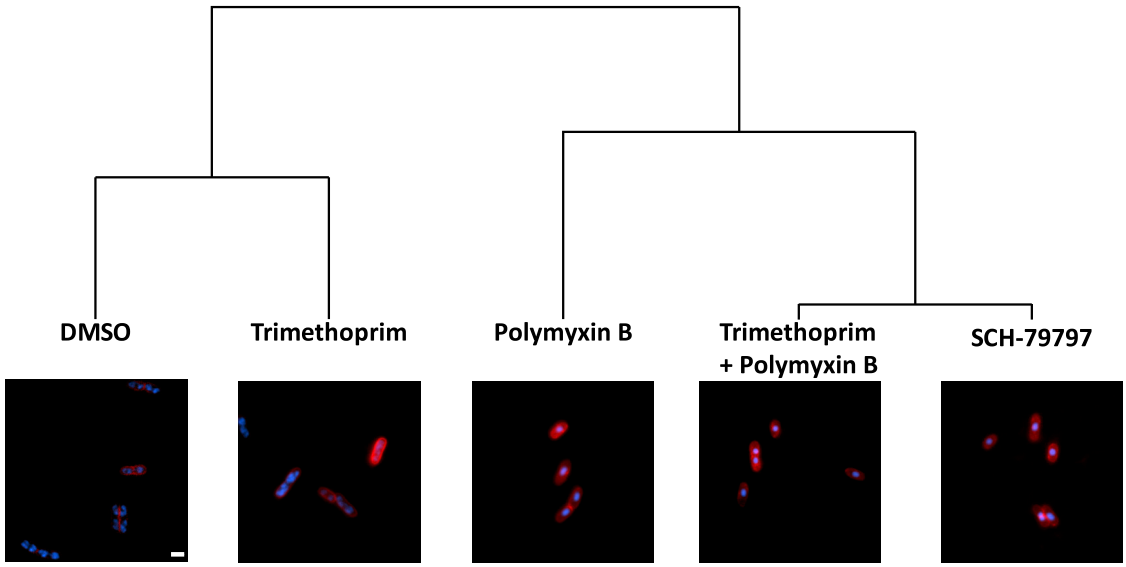

Figure S6. SCH-79797 Mimics Co-treatment with Folate Metabolism and Alternate Membrane Integrity Disruptors, Related to Figure 6

BCP analysis of *E. coli lptD4213* cells after 30 minutes of treatment with 1% DMSO, 6.3 μg/mL SCH-79797 (1X MIC), 2 μg/mL trimethoprim (10X MIC), 0.8 μg/mL polymyxin B (2X MIC), or the combination of 2 μg/mL trimethoprim (10X MIC) and 0.8 μg/mL polymyxin B (2X MIC). Cytological profiles were clustered by the first three principal components that account for at least 90% of the variance between samples. Cells were stained with DAPI, FM4-64, and SYTOX Green. Shown here are the merged images of DAPI (blue) and FM4-64 (red). Scale bar is 2 μm.

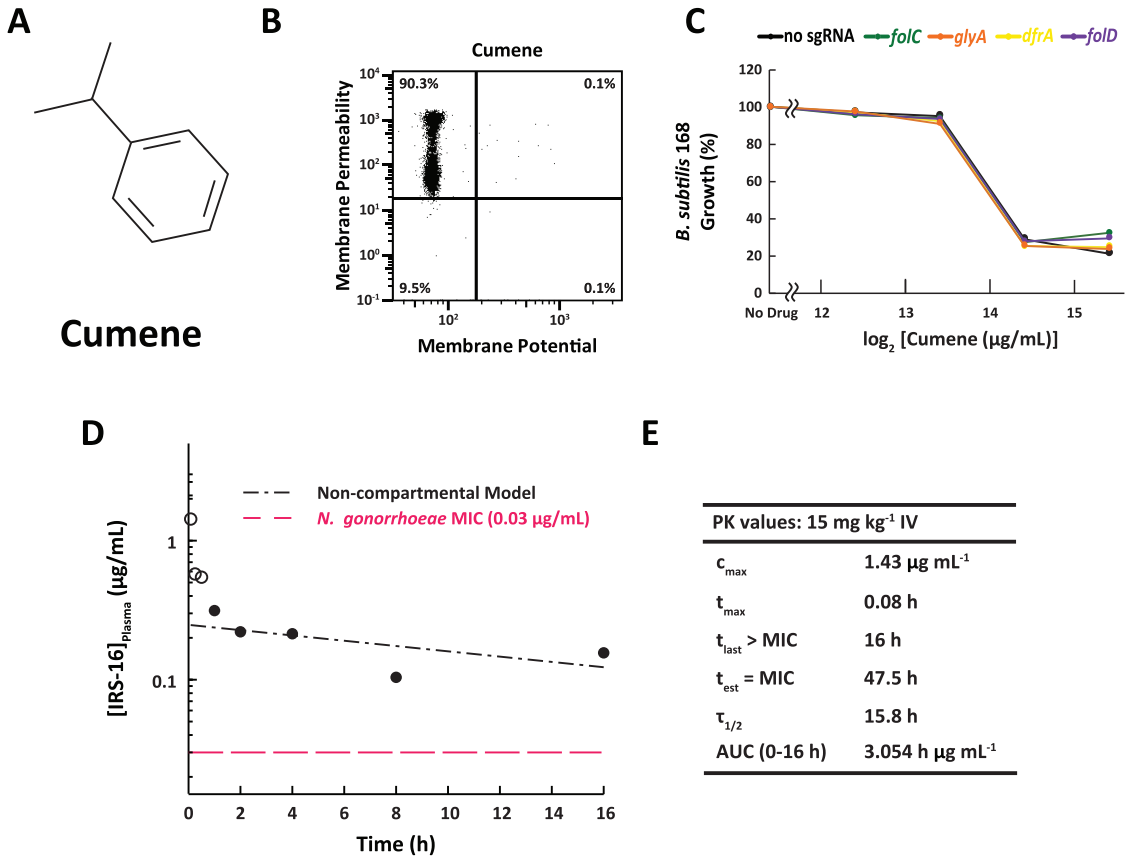

Figure S7. Cumene (Isopropylbenzene) Disrupts Membrane Integrity with No Additional Sensitivity in Folate-Metabolism Mutants and Pharmacokinetic Analysis of IRS-16 Stability, Related to Figure 7

(A) Structure of cumene. (B) Flow cytometry analysis of the membrane potential and permeability of *E. coli lptD4213* cells after 15 minute incubation with 17000 µg/mL cumene (1X MIC). The limits for the depolarized region were defined by comparing the values in the CCCP and solvent only controls. The limits for the permeabilized region were defined by comparing the nisin and solvent only controls. (C) The growth of CRISPRi *B. subtilis* knockdown mutants relative to a DMSO-treated control after cumene treatment. Bacterial growth was measured for 14 h and the final optical density (OD_{600}) of each condition was plotted against drug concentration. (D) Plasma concentrations of IRS-16 were measured following a single 15000 µg/kg IV dose. After the rapid initial approach to pseudoequilibrium, filled data symbols were used as the input for terminal half-life determination. (E) Pharmacokinetic parameters estimated of a non-compartmental model of IRS-16 serum levels.